

MEASUREMENT BY USE OF THE ROTATING CYLINDER TECHNIQUE
OF THE RATE OF THE SOLUTION OF WINTERVELD CHROMITE
ORE IN SLAG.

by Edwin Harm Roos

A dissertation presented to the Faculty of Engineering,
University of the Witwatersrand, for the degree of
Master of Science in Engineering 1982

DECLARATION

I declare that this dissertation is my own, unaided work except for chemical and microprobe analysis done by the Analytical and Mineralogy Divisions of the National Institute for Metallurgy. It is being submitted for the degree of Master of Science in the University of the Witwatersrand, Johannesburg. It has not been submitted for any degree or examination in any other University.

Edwin Harm Roos

30th day of June 1981.

To my loving wife
Desiree Dehola Roos

To my loving wife
Desiree Dehola Ross

ABSTRACT

In this investigation a relatively new technique for pyrometallurgy - the rotating cylinder technique - was used to investigate the dissolution rate of chromite ore in the slag.

The chromite ore dissolves very slowly but agglomerates of chromite grains have the tendency to fall apart at higher temperatures (1700° C and higher). This latter effect produces a suspension of chromite grains in the slag, thus enhancing the dissolution rate by its larger surface contact area with slag.

During the dissolution process, chromium and iron ions diffuse out of the reaction rim surrounding individual chromite grains into the slag, aluminium and magnesium ions diffuse from the slag into this layer. An 'inert' layer around the chromite grains is thus formed which prevents fast dissolution in the slag.

Pieces of this reaction layer have the tendency though to break off due to the drag forces exerted on it by viscous flow of the slag.

Preface

The National Institute of Metallurgy who subsidized this investigation makes great efforts to understand the processes involved in ferrochrome furnaces using South African chromites.

This investigation looks at the dissolution of chromite in slag. This is an important phenomenon during the production of ferrochrome. The production of ferrochrome from chromite ore and coal consists of many steps, of which several could be rate determining. The dissolution of chromite is one of the possible rate determining steps.

It is therefore, from a production point of view, important to know which factors effect the dissolution rate and to know what its magnitude is.

Previously I have been involved in a preliminary investigation on the use of organic binders in chromite pellets which gave me background information about the problems involved in the production of ferrochrome.

I would like to thank Dr Finn for his advice and guidance during this investigation.

LIST OF CONTENTS

	<u>page</u>
1 INTRODUCTION	
1.1 General.....	1
1.2 Previous work.....	2
2 THEORETICAL DEVELOPMENT	
2.1 Chromite.....	3
2.1.1 Mineralogy.....	3
2.1.2 Structure and Diffusion.....	3
2.2 Slags.....	7
2.2.1 Slag chemistry and structure....	7
2.2.2 Diffusion in slags.....	11
2.2.3 Viscosity of slags.....	6
2.2.4 Transport of ions dissolved in the presence of flow.....	19
3 EXPERIMENTAL PROCEDURES AND TECHNIQUES	
3.1 Rotating cylinder technique.....	24
3.2 Furnace types.....	24
3.3 Dissolution experiments.....	29
3.4 Microprobe, electron microscope and optical microscope work.....	33
4 RESULTS	
4.1 Quantitative results.....	34
4.2 Qualitative results.....	40
5 DISCUSSION.....	49
6 CONCLUSIONS.....	59
7 APPENDIXES.....	62
8 REFERENCES.....	72
9 ACKNOWLEDGEMENTS.....	78
10 RECOMMENDATIONS FOR FUTURE WORK.....	79

List of Tables

	<u>page</u>
<u>1.</u> Diffusion coefficients for various spinels.	5
<u>2.</u> Approximate diffusion coefficients of chromite at various temperatures.	6
<u>3.</u> Classification of cations according to their field strengths.	8
<u>4.</u> Types of molecules present in the slag at different SiO ₂ /MO ratios.	9
<u>5.</u> Slag compositions used in ferro-chrome production.	10
<u>6.</u> Slag analysis.	11
<u>7.</u> Estimated diffusion coefficient for various constituents in a slag.	16
<u>8.</u> Slag compositions for viscosity measurement used by Ossin (24).	18
<u>9.</u> Viscosities of three slags at 1550°, 1600°, 1650° and 1700°C.	19
<u>10.</u> Chemical analysis of slag before and after dissolution experiments.	34
<u>11.</u> Electron microprobe analysis for the bulk of the chromite and the reaction rim.	36
<u>12.</u> Ratios for various oxides of the bulk of the chromite and the reaction rim.	48
<u>13.</u> Average mass fluxes of iron ions from the chromite cylinder to the slag.	52
<u>14.</u> The mass transfer coefficient for different values of peripheral speed and temperature.	52
<u>15.</u> Reynolds numbers at 1550°, 1600°, 1650° and 1700°C.	53

List of Tables

	<u>page</u>
<u>1.</u> Diffusion coefficients for various spinels.	5
<u>2.</u> Approximate diffusion coefficients of chromite at various temperatures.	6
<u>3.</u> Classification of cations according to their field strengths.	8
<u>4.</u> Types of molecules present in the slag at different SiO ₂ /MO ratios.	9
<u>5.</u> Slag compositions used in ferro-chrome production.	10
<u>6.</u> Slag analysis.	11
<u>7.</u> Estimated diffusion coefficient for various constituents in a slag.	16
<u>8.</u> Slag compositions for viscosity measurement used by Ossin (24).	18
<u>9.</u> Viscosities of three slags at 1550°, 1600°, 1650° and 1700°C.	19
<u>10.</u> Chemical analysis of slag before and after dissolution experiments.	34
<u>11.</u> Electron microprobe analysis for the bulk of the chromite and the reaction rim.	36
<u>12.</u> Ratios for various oxides of the bulk of the chromite and the reaction rim.	48
<u>13.</u> Average mass fluxes of iron ions from the chromite cylinder to the slag.	52
<u>14.</u> The mass transfer coefficient for different values of peripheral speed and temperature.	52
<u>15.</u> Reynolds numbers at 1550°, 1600°, 1650° and 1700°C.	53

	<u>page</u>
<u>16.</u> Densities and FeO% values for the reaction rim.	55
<u>17.</u> Average composition (FeO) of the slag during the various experiments (mass percent).	55
<u>18.</u> Concentration gradients over the interface chromite slag for various percentages of FeO in the chromite and the mass fluxes as result of the gradients.	54
<u>19.</u> Mass fluxes due to diffusion at various temperatures and reaction rim thickness.	57
<u>20.</u> The composition of chromite and reaction rim and the mass fluxes necessary to convert chromite to reaction rim (For various conversion factors)	71

List of Figures

	<u>page</u>
<u>1.</u> Tracer diffusivity of Ca^{45} in $\text{CaO} - \text{SiO}_2$ melts as a function of the temperature.	13
<u>2.</u> Diffusivity of Ca^{45} as a function of the molefraction of silica for 1600°C .	13
<u>3.</u> Chemical diffusion of Ca^{2+} ions into the eutectic slag of composition 38% $\text{CaO} - 20\% \text{Al}_2\text{O}_3 - 42\% \text{SiO}_2$.	14
<u>4.</u> Diffusion of silicon in the lime-alumina-silica system.	14
<u>5.</u> A molybdenum wound furnace with a rotating cylinder.	25
<u>6.</u> A molybdenum crucible, slag and rotating cylinder.	32
<u>7.</u> Percentage iron dissolved in a slag plotted against time, at various temperatures.	35
<u>8.</u> Rates of dissolution of iron ions, coming from Winterveld chromite, into a slag.	37
<u>9.</u> Concentration profiles for Cr, Fe, Al and Mg over chromite, reaction rim and slag.	38
<u>10.</u> Temperature profiles of a molybdenum wound furnace.	51

List of Plates

	<u>page</u>
<u>1.</u> The chromite cylinder before and after dissolution.	30
<u>2.</u> Chromite, reaction rim and slag, 30 min, 1650°C.	41
<u>3.</u> Chromite, reaction rim and slag, 10 min, 1720°C.	41
<u>4.</u> Chromite and gangue bands, 30 min, 1650°C.	42
<u>5.</u> Electron micrograph of chromite, reaction rim and slag, 1 hr, 1600°C.	43
<u>6.</u> Distribution of Cr.	44
<u>7.</u> Distribution of Fe.	44
<u>8.</u> Distribution of Al.	44
<u>9.</u> Distribution of Mg.	44
<u>10.</u> Electron micrograph of chromite and reaction rim, 1 hr, 1600° C.	45
<u>11.</u> Distribution of Cr.	45
<u>12.</u> Distribution of Al.	46
<u>13.</u> Distribution of Mg.	46
<u>14.</u> Chromite with a gangue band, 1 hr. 1600°C.	46
<u>15.</u> Distribution of Cr.	47
<u>16.</u> Distribution of Mg.	47
<u>17.</u> Distribution of Si.	47

List of Symbols

a	Ionic distance
B	Thermal expansion coefficient
C	Concentration
C _p	Heat capacity
D _a	Diffusion constant
D _{Fe}	Diffusion coefficient of Fe
d	Thickness boundary
E _d	Activation energy
g _x	Gravitational constant
J	Total Mass flux
k	Mass transfer coefficient
l	Characteristic dimension
n	Dynamic viscosity
n _x	Mass flux in the x-direction
N _{PL}	Prandtl number
N _{sc}	Schmidt number
N _{Gr}	Grashof number
P	Density
R	Gas constant
Re	Reynolds number
r	Ionic radius
T	Absolute temperature
→T _{yx}	Shear force
u	Peripheral speed
v	Kinematic viscosity
v _x	Velocity in the x-direction
x	Distance
Z	Ionvalency

1 INTRODUCTION

1.1 General

The properties of chromite under various conditions have been investigated extensively by various writers (7,17,18,19). Also the physico-chemical properties of slag under various conditions and the influence of FeO and Cr_2O_3 thereupon have been investigated by many. (1,2,3,4,5,7,17) All these investigations have been directed towards understanding the behaviour of South African chromite ores during ferro-chromium production in a submerged arc furnace and thus to be able to enhance the productivity of the furnaces and the quality of the produced ferrochromium.

This work covers a missing link in these investigations, the interaction of chromite and slag at high temperatures (1550° - 1700°). Only one writer (17) has done some work in this field. It was felt though that more work is needed to give a better idea of the rates of dissolution and the mechanisms that are involved during the dissolution. The writer feels that this work certainly answers some of the questions about the dissolution rate and the mechanisms of dissolution of chromite ore in a slag. It raises a few questions about the mechanisms as well.

1.2 Previous Work

Urquhart (17) did some work on the dissolution of chromite. Although this work was a minor part of this thesis, some was directed toward finding the importance of the dissolution rate of chromite ore in a slag on the rate of reduction.

However, many dissolution curves of chromite ore in the slag were obtained by him.

It is clear from his data and his evaluation that the dissolution process is not simply a chemical attack of the chromite ore by the slag. This makes it difficult to give exact data on the dissolution rate. The chemical analysis of the slag will show the combined effects of dissolution and particles in suspension.

The reduction of chromite via the slag phase is for obvious reasons also affected by these two effects. Any measurement of the reduction rate which does not consider both effects will give erroneous results and conclusions.

2 THEORETICAL DEVELOPMENT

2.1 Chromite

2.1.1 Minerology of Chromite

Chromite belongs to the spinel group of minerals. It has the common formula of $(Mg^{2+}, Fe^{2+})_O (Cr^{3+}, Al^{3+}, Fe^{3+})_2 O_3$. Chromite ore is actually a solid solution of several spinels $FeCr_2 O_4$, $Fe Fe_2 O_4$, $MgCr_2 O_4$, $MgAl_2 O_4$, $MgFe_2 O_4$ and $Fe Al_2 O_4$. In most cases chromite contains the following elements as well: Ti, V, Mn, Ni, to about 1%. InO , NiO and $V_2 O_5$ are part of the spinel structure, while TiO_2 is part of the ulvospinel structure.

Chromite as a concentrate always contains a certain percentage of gangue material like clinopyroxene and others. Winterveld chromite as used in this investigation has a density of 4.4 gr/cm^3 . The chemical analysis is as follows (Electron microprobe analysis NIM): $Cr_2 O_3$ 48.18%, FeO 24.7%, MgO 11.29%, $Al_2 O_3$ 13.55%, MnO 0.35%, SiO_2 0.03%, CaO 0.01%, TiO_2 0.84%.

2.1.2 Structure and diffusion

The basic cell of chromite contains 56 ions of which 32 are oxygen in a close cubic packing. The holes between the oxygen ions contain two types of cations; eight with a fourfold coordination, tetrahedral sites, and sixteen with a sixfold coordination, octahedral sites. There are two kinds of cation/oxygen layers.

- 1) Oxygen ions and cations with sixfold coordination and fourfold coordination
- 2) Oxygen ions and cations with only sixfold coordination.

Both layers are close cubic packed.

The chromite structure also contains many octahedral and tetrahedral vacancies. Taking AB_2O_3 as the overall formula for the chromite spinel, then the B-Ions are on the octahedral sites while the A-Ions are on the tetrahedral sites.

Grimes (41) describes in detail the diffusion path of cations in spinels. Because each cation is surrounded by many vacant tetrahedral and octahedral sites, there are basically two routes open for migration: A cation occupying a tetrahedral site (Fe^{2+} in chromite for instance) could jump to one of six nearest similar tetrahedral sites or one of four nearest octahedral sites. In fact, according to Grimes the migration of the divalent ions Co^{2+} , Ni^{2+} and Zn^{2+} in spinel has unambiguously been identified with the route via alternating octahedral and tetrahedral sites.

A cation in an octahedral site (Cr^{3+} for instance) can diffuse by migrating via octahedral sites only, or by migrating first to one of eight neighbouring vacant tetrahedral sites and then to a vacant octahedral site. According to Grimes the Cr^{3+} ions mostly diffuse in the last manner but this is probably combined with diffusion via octahedral sites only.

According to Evans (13) the alumina content can gradually increase through substitution of Fe by Al. The electrical neutrality is achieved simply by the appearance of vacant sites in positions which would normally be occupied by cations. Other possibilities for diffusion are grain boundaries and external surfaces, these being regions of high disorder. These areas contain a higher concentration and a wider variety of defects than the bulk material and provide thus lower energy saddle

points for migration of defects. In solids the magnitude and temperature dependence of the diffusion coefficient depend first on the concentration of lattice defects (vacancies or interstitial ions) which are capable of contributing to the diffusivity. It is also dependant on the energy required for movement of these defects through the lattice.

Generally data on diffusion in solids are very scarce. I found no data on the diffusion in chromites. Thus an evaluation of diffusion coefficients of spinels had to be done in order to give an estimate of the diffusion coefficient in chromite, belonging to the spinel group as well. This data have to be treated with care of course. They can serve only as an indication of the order of magnitude of the diffusion coefficients of chromite at various temperatures. The temperature dependence of the diffusion coefficient can be expressed at (9, 10, 23):

$$D = D_0 e^{-E_d/RT} \quad (1)$$

D = Diffusion coefficient at temperature T cm²/sec

D₀ = Diffusion constant cm²/sec

T = Absolute temperature K

R = Gas constant 1,987 cal K.mole

E_d = Activation energy cal/mole

This formula is used to calculate the diffusion coefficients at 1550° and 1700° C from the data presented in Table 1 (20).

Table 1 : Diffusion coefficients of various compounds by Elliott (20)

	Diffusing Species	Medium	Temperature °C	D_0 cm ² /sec	D_d cal/mole	Ref.
a	Co	CoCr ₂ O ₄	1400 - 1600	10 ⁻³	51,000	(35)
b	Cr	CoCr ₂ O ₄	1400 - 1600	2	70,000	(35)
c	Ni	NiCr ₂ O ₄	800 - 1300	1,5.10 ⁻³	61,400	(36)
d	Cr	NiCr ₂ O ₄	950 - 1700	0,74	72,500	(37)
e	Fe	Fe ₃ O ₄	750 - 1000	5,2	55,000	(38)

The values for the diffusion of Cr in b and d are of the same order of magnitude. I chose the value obtained with CoCr₂O₄ as the best one since it has been measured at higher temperatures.

The values for the diffusion of Fe can be approximated by the diffusion of Co and Ni. The value of cobalt seems to be the best one because the radius of Co²⁺ is very close to the radius of Fe²⁺ (0,72Å versus 0,74Å) while Ni²⁺ has a radius of 0,69 Å.

If these values are used to calculate the diffusion coefficients of Fe and Cr in chromite at various temperatures the following results are obtained (Table 2).

Table 2 : Approximate diffusion coefficients of Fe²⁺ and Cr³⁺ in chromite at 1550°C, 1600°C, 1650°C and 1700°C.

Temperature °C	D_{Fe} (act. D_{Co}) cm ² s ⁻¹	D_{Cr} cm ² s ⁻¹
1550	7,7.10 ⁻¹⁰	8,1.10 ⁻⁹
1600	1,1.10 ⁻⁹	1,4.10 ⁻⁸
1650	1,6.10 ⁻⁹	2,2.10 ⁻⁸
1700	2,3.10 ⁻⁹	3,5.10 ⁻⁸

2.2 Slags

2.2.1 Slag chemistry and structure

The slag chemistry and its structure are described in great detail in other works (2,3,4,8,11,24). Only an extract of the most important facts is given.

A slag is a mixture of network forming components and network breaking components. The differences in co-ordination of various components show that the cation-oxygen bonds are considerably stronger in the acid than in the basic oxides (Table 3).

Element	Valency z	Ionic radius r	Ionic distance a	Coord. no.	Field Strength at distance 'a' from anion z/a^2
K	1	1.33	2.65	8	0.13
Na	1	0.98	2.30	6	0.19
Li	1	0.78	2.10	6	0.23
Ba	2	1.43	2.75	8	0.24
Pb	2	1.32	2.64	8	0.27
Sr	2	1.27	2.59	8	0.28
Ca	2	1.06	2.38	8	0.33
Mn	2	0.91	2.23	6	0.40
Fe	2	0.83	2.15	6	0.43
Zn	2	0.83	2.15	4	0.49
Mg	2	0.78	2.10	6	0.45
				4	0.53
Zr	4	0.87	2.19	8	0.77
Be	2	0.34	1.66	4	0.85
Fe	3	0.67	1.99	6	0.76
				4	0.85
Al	3	0.57	1.89	6	0.84
				4	0.96
Ti	4	0.64	1.96	6	1.04
B	3	0.20	1.52	4	1.34
				3	1.63
Si	4	0.39	1.71	4	1.57
P	5	0.24	1.66	4	2.10

Table 3 Classification of cations according to their field strengths, $\frac{z}{a^2}$, after Dietzel (39)

With progressive additions of basic oxides the three dimensional structure is steadily broken down until the silica is present as discrete SiO_4^{4-} groups (Table 4).

Table 4. Type of ions present in slag at different SiO_2/MO ratios (40)

Composition	Molar % Oxide	Discrete Ion	Description
$2\text{MO} \cdot \text{SiO}_2$	66	$(\text{SiO}_4)^{4-}$	Type A
$3\text{MO} \cdot 2\text{SiO}_2$	60	$(\text{Si}_2\text{O}_7)^{6-}$	Basic Tetrahedron
$4\text{MO} \cdot 3\text{SiO}_2$	57	$(\text{Si}_3\text{O}_{10})^{8-}$	Type B
$5\text{MO} \cdot 4\text{SiO}_2$	55	$(\text{Si}_4\text{O}_{13})^{10-}$	Linear Polymerisation
$6\text{MO} \cdot 5\text{SiO}_2$	54	$(\text{Si}_5\text{O}_{16})^{12-}$	"
$11\text{MO} \cdot 10\text{SiO}_2$	52	$(\text{Si}_{10}\text{O}_{31})^{22-}$	"
$\text{MO} \cdot \text{SiO}_2$	50	$(\text{Si}_3\text{O}_9)^{6-}$	"
$\text{MO} \cdot 2\text{SiO}_2$	33	$(\text{Si}_6\text{O}_{15})^{6-}$	"
$\text{MO} \cdot 3\text{SiO}_2$	25	$(\text{Si}_9\text{O}_{21})^{6-}$	Type C
$\text{MO} \cdot 4\text{SiO}_2$	20	$(\text{Si}_{12}\text{O}_{27})^{6-}$	Ring Structure
$\text{MO} \cdot 5\text{SiO}_2$	16.7	$(\text{Si}_{15}\text{O}_{33})^{6-}$	"
$\text{MO} \cdot 6\text{SiO}_2$	14.3	$(\text{Si}_{18}\text{O}_{39})^{6-}$	"
$\text{MO} \cdot 7\text{SiO}_2$	12.5	$(\text{Si}_{21}\text{O}_{51})^{6-}$	"
$\text{MO} \cdot 8\text{SiO}_2$	11.1	$(\text{Si}_{24}\text{O}_{51})^{6-}$	"

Depending on the concentration and the character of the oxide, a number of bonds will be broken. This has a significant effect on the viscosity of the slag. The conductance as well as the diffusion in the slag is dependant on the oxygen ion concentration.

The viscosity of the melt decreases rapidly as the three dimensional structure is disrupted. The viscosity-composition relation is non-linear. A reason for this is that intermediate compounds are formed during the progressive addition of basic oxides (Table 4). The structure of the slag can be compared with that of a glass i.e. it has a short range order but no long range order as in crystals.

A large variety of slag compositions is used in the ferrochrome production (Table 5).

Table 5: Slag compositions according to various sources used in the ferrochrome production.

	% SiO ₂	% MgO	% Al ₂ O ₃	% CaO
Robiette (12)	30	30	30	
Urquhart (17)	50	32	28	
Volkert (25)	29-32	32-35	29-32	3,5-6

(% = mass percent)

For the experiments described in this work a slag was chosen with a low liquidus temperature (about 1500°C) which has also a composition close to the compositions mentioned in Table 5.

The result of this work can therefore be compared with conditions existing in slags normally used in South Africa for the ferrochrome production. The composition of the slag used is:

SiO ₂	MgO	Al ₂ O ₃	CaO
45%	29%	18%	8%

Analysis done on the slag show there was about 0,35% FeO present in the second batch (Table 6). The first batch was not analysed for iron but is assumed to have the same percentage of iron oxide, because it was made in an identical way as the second batch using the same materials.

Table 6 Slag analysis (mass percentages)

SiO ₂	MgO	Al ₂ O ₃	CaO	FeO
29	18,3	8,3	Not analysed	
29,2	18,0	8,5	0,35	

... in composition are neglected in ... and in the discussion. The slag had, ... us temperature of 1520°C, ... tage microscope. ($P_{O_2} = 4 \times 10^{-5}$ atm)

Diffusion

... defined as a transport process of ... due to thermally activated motion ... molecules. Material fluxes due to ... can be described with the following ... first law:

$$J = -D \frac{dc}{dx} \quad (2)$$

J Flux (moles/cm²/sec)

D Diffusion coefficient (cm²/sec)

c Concentration (moles/cm³)

x Distance over which the diffusion takes place (cm).

Fick's second law is concerned with changes in concentration with time:

$$\frac{dc}{dt} = \frac{d}{dx} \left(D \frac{dc}{dx} \right) \quad (3)$$

If D is assumed constant and it varies only slightly with the composition,

$$\frac{dc}{dt} = D \frac{c^2}{c^2 x} \quad (4)$$

is valid. The temperature dependence described by an Arrhenius plot:

$$D = D_0 e^{-E_d/RT} \quad (1).$$

This is the same formula as the one for the solid state diffusion.

Not many data are available about self-diffusion coefficients in slags measured by radioactive tracing methods (16,21,22). Experimental data obtained indicate that the diffusion coefficients under a chemical concentration gradient are not significantly different from self diffusion coefficients. Therefore, self-diffusion coefficients can be used in mass transfer correlations.

Taylor (21) mentions that Ca and Si diffusion coefficients vary little if at all with the slag composition at least for a slag containing a fair amount of silica, at least 40%. Figures 1,2,3 and 4 show some data of diffusion coefficients of various compounds in slags. The latest data (16) on the diffusion of Ca^{2+} in $CaO-SiO_2$ melts indicate a dependence on the molefraction of SiO_2 . This is contrary to Taylor's remark (21) that there is no such dependence. Because the slag used in this work contained a significant amount of Al_2O_3 (18.3%), the data obtained by Taylor are thought to be more valid, which are from

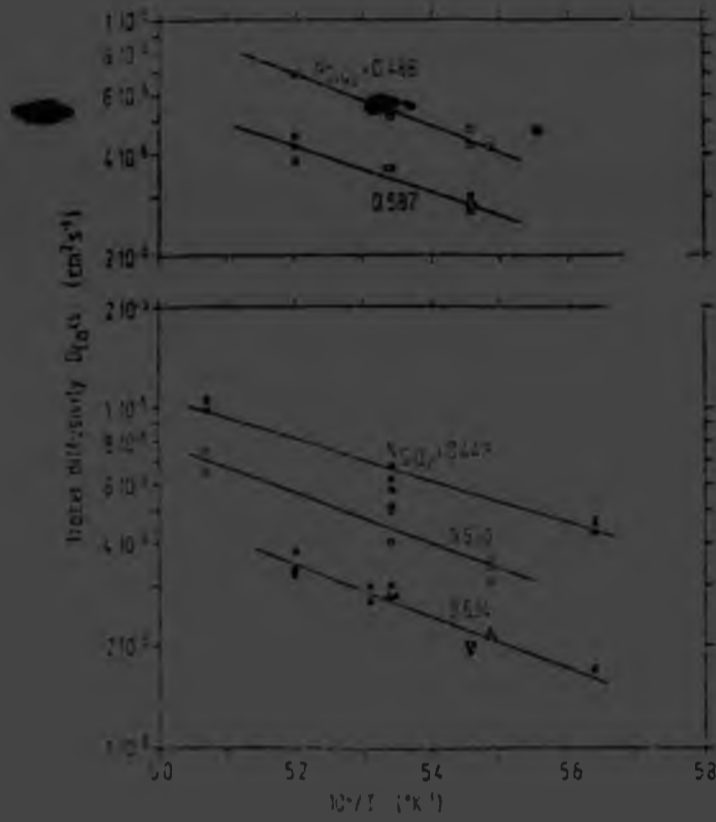


Fig.1 (16) Tracer diffusivity of Ca^{45} in $CaO-SiO_2$ melts as a function of temperature.

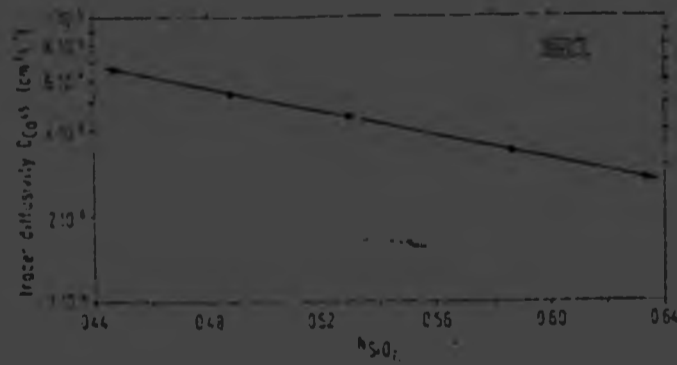


Fig. 2 (16) Tracer diffusivity of Ca^{45} as a function of mole fraction of silica for 1600°C.

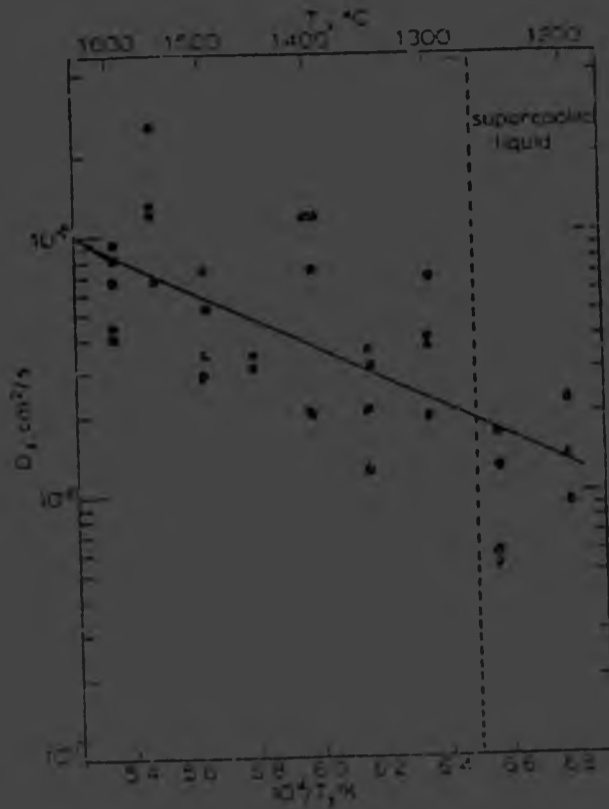


Fig.3 (21) Chemical diffusion of Ca^{45} ions introduced as Ca^{45}O into the eutectic slag of composition $38\% \text{CaO}-20\text{Al}_2\text{O}_3-42\text{SiO}_2$

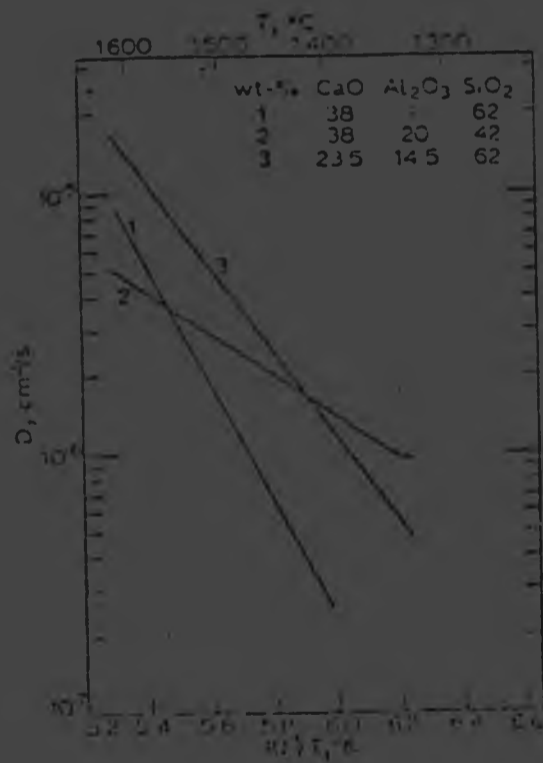


Fig.4 (21) Diffusion of silicon in the lime-alumina-silica system.

melt containing 20%Al₂O₃, 42%SiO₂, 38%CaO (Fig.3). The data in Table 7 for D_{Ca} are taken from Figure 3. The data for the other diffusivities are calculated according to the statement of Taylor that the diffusion coefficient of Al³⁺ and Si⁴⁺ is approximately half of Ca²⁺, while the diffusion coefficient for the Fe²⁺ is about twice as large as for Ca²⁺.

It is assumed that the behaviour of Cr³⁺ is similar to that of Al³⁺ and the behaviour of Mg²⁺ is similar to that of Ca²⁺ as no data is available for these ions.

Table 7
Diffusion coefficients of various species in slag
at different temperatures (cm²/sec)

	50°C	1600°C	1650°C	1700°C
D _{Ca} =	7x10 ⁻⁶	8x10 ⁻⁶	1x10 ⁻⁵	1,4x10 ⁻⁵
D _{Mg} =	7x10 ⁻⁶	8x10 ⁻⁶	1x10 ⁻⁶	1,4x10 ⁻⁵
D _{Fe} =	1,4x10 ⁻⁵	1,6x10 ⁻⁵	2x10 ⁻⁵	2,8x10 ⁻⁵
D _{Al} =	3,5x10 ⁻⁶	4x10 ⁻⁶	5x10 ⁻⁶	7x10 ⁻⁶
D _{Si} =	3,5x10 ⁻⁶	4x10 ⁻⁶	5x10 ⁻⁶	7x10 ⁻⁶
D _{Cr} =	3,5x10 ⁻⁶	4x10 ⁻⁶	5x10 ⁻⁶	7x10 ⁻⁶

These data must be seen only as estimations which are useful for the purpose of this work.

2.2.3 Viscosity of slags

The viscosity of slags is examined in this work from the viewpoint of transport kinetics. The relation between these two concepts is rather obvious if one considers that a flow is actually transport of mass and momentum.

The viscosity is a measure for an amount of momentum transfer between two layers in a moving fluid. Two layers in a fluid moving in the same direction but with a different velocity, will exert a shear force on each other causing the fluid to have a velocity gradient between the two layers. This shear force is a direct result of momentum transfer and is proportional to the velocity gradient and the viscosity of the fluid.

$$T_{yx} = -n \frac{dv_x}{dy} \quad (5)$$

v_x = velocity in the x- direction cm/sec

T_{yx} = shear force in the x- direction on a plane of constant y.

n = dynamic viscosity g/cm.sec

The kinematic viscosity at a certain temperature is the dynamic viscosity divided by the density of the slag at that temperature.

$$v = \frac{n}{p} \quad (6)$$

v = kinematic viscosity (stokes)

n = dynamic viscosity g/cm.sec

p = density g/cm³

The viscosity of slags diminishes with increasing temperature, this relation is often expressed with the following formula.

$$\log n = a + b \left(\frac{1}{T} \right) \quad (7)$$

n = dynamic viscosity g/cm.sec

T = absolute temperature K

a and b are constants

$$T_{yx} = -n \frac{dv_x}{dy} \quad (5)$$

v_x = velocity in the x- direction cm/sec

T_{yx} = shear force in the x- direction on a plane of constant y.

n = dynamic viscosity g/cm.sec

The kinematic viscosity at a certain temperature is the dynamic viscosity divided by the density of the slag at that temperature.

$$v = \frac{n}{\rho} \quad (6)$$

v = kinematic viscosity (stokes)

n = dynamic viscosity g/cm.sec

ρ = density g/cm³

The viscosity of slags diminishes with increasing temperature, this relation is often expressed with the following formula.

$$\log n = a + b \left(\frac{1}{T} \right) \quad (7)$$

n = dynamic viscosity g/cm.sec

T = absolute temperature K

a and b are constants

Table 8. Slag compositions for viscosity measurements.

(Weight percentages)	SiO ₂	MgO	AlO ₃	CaO
A6	45	26	20	8,9
A10	40	29,9	20	9,9
Inis work	45	29,0	18,3	8,3

Many measurements of the viscosities of various slags used in ferrochrome production have been made in the past (1,2,3,24). It is important to know the viscosities of the slag melts at the temperature used in this work because of their role in the mass transfer correlations describing the transport of solute into the slag from the rotating cylinder.

There is a considerable difference in the measurements made by the various workers, sometimes more than a factor 10. No attempts were made to interpolate these data. Another way was followed to obtain reasonably accurate data. The latest values were taken (Ossin 24). Two measurements by Ossin of the viscosity of two slags with a composition close to the composition of the slag used in this work were used and interpolated. The slag compositions used were A6 and A10 from Ossin (24).

The viscosity (η) depends among others on the ratio of the network forming compounds and the network breaking compounds ($\text{SiO}_2 + \text{Al}_2\text{O}_3 / \text{MgO} + \text{CaO}$). This ration is used to determine the position of the slag used in relation to A₆ and A₁₀:

Ratio A₆ : 1,86
Ratio A₁₀ : 1,51
Ratio this work : 1,70.

This small calculation shows that the viscosity of the slag used in this work can be taken halfway between the values for A_6 and A_{10} .

Ossin gives the following values for η (poises) as a function of temperature:

Table 9. Viscosities of three slags at various temperatures.

	Temperature			
	1550°C	1600°C	1650°C	1700°C
		Viscosity(poise)		
A_6	5,16	3,8	2,9	2,2
A_{10}	2,9	2,3	1,8	1,4
This work	4,03	3,05	2,35	1,8

By taking the values for the slag used in this work halfway those of A_6 and A_{10} we get the values in the bottom row.

2.2.4 Transport in the slag in the presence of flow.

All literature (4, 24, 25, 26) agrees on the large amount of energy that is dissipated just above the slag level by the electrodes of the furnace. This energy is transported via the slag to the metal bath and other parts of the furnace. This transport of thermal energy takes place through thermal conduction,

radiation and combined mass and thermal transport.

Massflow in the slag layer is induced through several factors.

- 1) When chromite ore is reduced around the electrode tips, a large volume of gases like CO, CO₂ and SiO flow away from this region. This flow will stir the slag layer.
- 2) Reduction processes take place in the slag layer. These evolve gases which stir the slag layer as well.
- 3) A thermal gradient exists between the metal bath and the top of the slag and also between the middle of the furnace and the furnace walls. These temperature differences within the slag layer cause the slag to have different densities at different places within the slag layer, causing the slag to flow.

Flows induced by density differences in the slag can be characterised by the dimensionless groups of Grashof (N_{gr}) and Prandtl (N_{pr}). The Grashof number describes the ratio of buoyancy forces and viscous forces in the system

$$N_{gr} = \frac{g_x \cdot x^3 \cdot B \cdot (T_w - T_b)}{\nu^2} \quad (8)$$

- g_x = gravitational constant (cm/sec²)
 x = characteristic dimension (cm)
 B = thermal expansion coefficient (°C⁻¹)
 T_w = temperature of the hot spot (°C)
 T_b = temperature of the bulk (°C)
 ν = kinematic viscosity (Stokes = cm²/sec)

The Prandtl number describes the ratio of momentum diffusivity and thermal diffusivity.

$$N_{pr} = \frac{C_p \cdot \eta}{k} \quad (9)$$

C_p = heat capacity (cal/g °C)

η = dynamic viscosity (poises = g/cm sec)

k = thermal conductivity (cal/sec.cm.°C)

Jacob (27) defines the laminar and turbulent flow regimes due to natural convection as

$$\text{laminar } 2 \times 10^3 < N_{gr} \cdot N_{pr} < 150 \times 10^3$$

$$\text{turbulent } 300 \times 10^3 < N_{gr} \cdot N_{pr} < 3 \times 10^7$$

According to Hejja (26) the flow in the slag due to this factor is turbulent. Of course these calculations are not very accurate but they give a first approximation of the conditions existing in the slag layer of the submerged arc furnace. All factors together will give a strongly turbulent condition in the slag layer.

The mass transfer correlation under turbulent flow conditions for a rotating cylinder can be described (10,23) as

$$\dot{n} = 0,079 \cdot Re^{-0,3} \cdot Sc^{-0,644} \cdot u \cdot (C_i - C_b) \quad (10)$$

$$k = 0,079 \cdot Re^{-0,3} \cdot Sc^{-0,644} \cdot u \quad (11)$$

$$\dot{n} = k \cdot (C_i - C_b) \quad (12)$$

\dot{n} = flux (mass) (mole/cm²/sec)

u = the peripheral speed of the rotating cylinder
cm/sec

Re = Reynolds number (dimensionless)

Sc = Schmidt number (dimensionless)

C_i = the concentration of the dissolving species
at the interface chromite slag (mole/cm³)

C_b = the concentration in the bulk of the slag
(mole/cm³)

$$Re = \frac{u \cdot l}{\nu} \quad (13)$$

$$Sc = \frac{\nu}{D} \quad (14)$$

l = characteristic dimension of the system in this
case the diameter of the cylinder (cm)

ν = kinematic viscosity (cm²/sec)

D = diffusion coefficient (cm²/sec)

k = mass transfer coefficient (cm/sec)

According to references 10 and 23 the flow starts to
be turbulent between $Re = 10-15$

It is essential that turbulent conditions exist in
the system because in the case of strictly laminar flow,
the streamlines of the slag will be concentric with the
cylinder surface. In this case all transport will be
via diffusion as the streamlines are perpendicular to
the diffusion path.

According to the earliest classical theory (23),
the flux of solute from a rotating cylinder is given

u = the peripheral speed of the rotating cylinder
cm/sec

Re = Reynolds number (dimensionless)

Sc = Schmidt number (dimensionless)

C_i = the concentration of the dissolving species
at the interface chromite slag (mole/cm³)

C_b = the concentration in the bulk of the slag
(mole/cm³)

$$Re = \frac{u \cdot l}{\nu} \quad (13)$$

$$Sc = \frac{\nu}{D} \quad (14)$$

l = characteristic dimension of the system in this
case the diameter of the cylinder (cm)

ν = kinematic viscosity (cm²/sec)

D = diffusion coefficient (cm²/sec)

k = mass transfer coefficient (cm/sec)

According to references 10 and 23 the flow starts to
be turbulent between $Re = 10-15$

It is essential that turbulent conditions exist in
the system because in the case of strictly laminar flow,
the streamlines of the slag will be concentric with the
cylinder surface. In this case all transport will be
via diffusion as the streamlines are perpendicular to
the diffusion path.

According to the earliest classical theory (23),
the flux of solute from a rotating cylinder is given

simply by the product of the driving force and the diffusional resistance through the boundary layer.

$$\dot{n} = D(C_1 - C_b)/d \quad (15)$$

d = thickness of the boundary layer

The thickness of the boundary layer may be determined by using dimensionless groups in a manner completely analogous to heat transfer.

The value for a mass transfer coefficient depends on the geometry of the system, stirring conditions, the viscosity and density of the liquid and the diffusivity of the slag to which k applies.

$$\dot{n} = D.(C_i - C_b)/l.f(Re, Sc) \quad (16)$$

l = characteristic dimension of the system
(diameter of the rotating cylinder)

$$\text{and } k = \frac{D}{l}.f(Re, Sc)^{-1} \quad (17)$$

$$\text{while } k = u.0.079Re^{-0.3}.Sc^{-0.644} \quad (11)$$

$$\text{can be written as } k = u.g(Re, Sc)^{-1} \quad (18)$$

A dimension analysis shows that equation (17) is equivalent to (18):

$$u \quad \text{cm/sec}$$

$$D/l \quad \frac{\text{cm}^2/\text{sec}}{\text{cm}} = \text{cm/sec}$$

3 EXPERIMENTAL PROCEDURES AND TECHNIQUES

3.1 Rotating Cylinder Technique

An experimental technique was chosen, that is often used in the hydro metallurgy to determine reaction rates at different peripheral speeds. Data obtained with this technique give insight on the influence of the flow rate of the liquid on the reaction at the rotating surface. This system has also more in common with the circumstances that prevail in the slag layer of the submerged arc furnaces, if compared with a stationary setup as used by Urquhart (17).

As discussed in 2.2.4 turbulent flow conditions prevail in the slag layer if cylinder exceeds a certain speed. This speed depends on the viscosity of the slag. This technique has recently been used successfully in pyrometallurgical research (28 & 31) although the temperatures that were used were significantly lower than in this work. This technique can give information about the dissolution mechanism and the rate controlling step of chromite solution in molten slag.

3.2 Furnace Types

The following apparatus were used in the experiments described in this work. A molybdenum wound furnace (figure 5) consisting of about 22 metres of 1 mm molybdenum wire which is wound around a tabular alumina tube (outside diameter 7,5 cm). The molybdenum winding has at room temperature a total resistance of about 2 Ohms. The current is supplied with a Eurotherm controller with a 25 Amp thyristor. The temperature of

FIGURE 5.
Molybdenum wound furnace with
a rotating cylinder

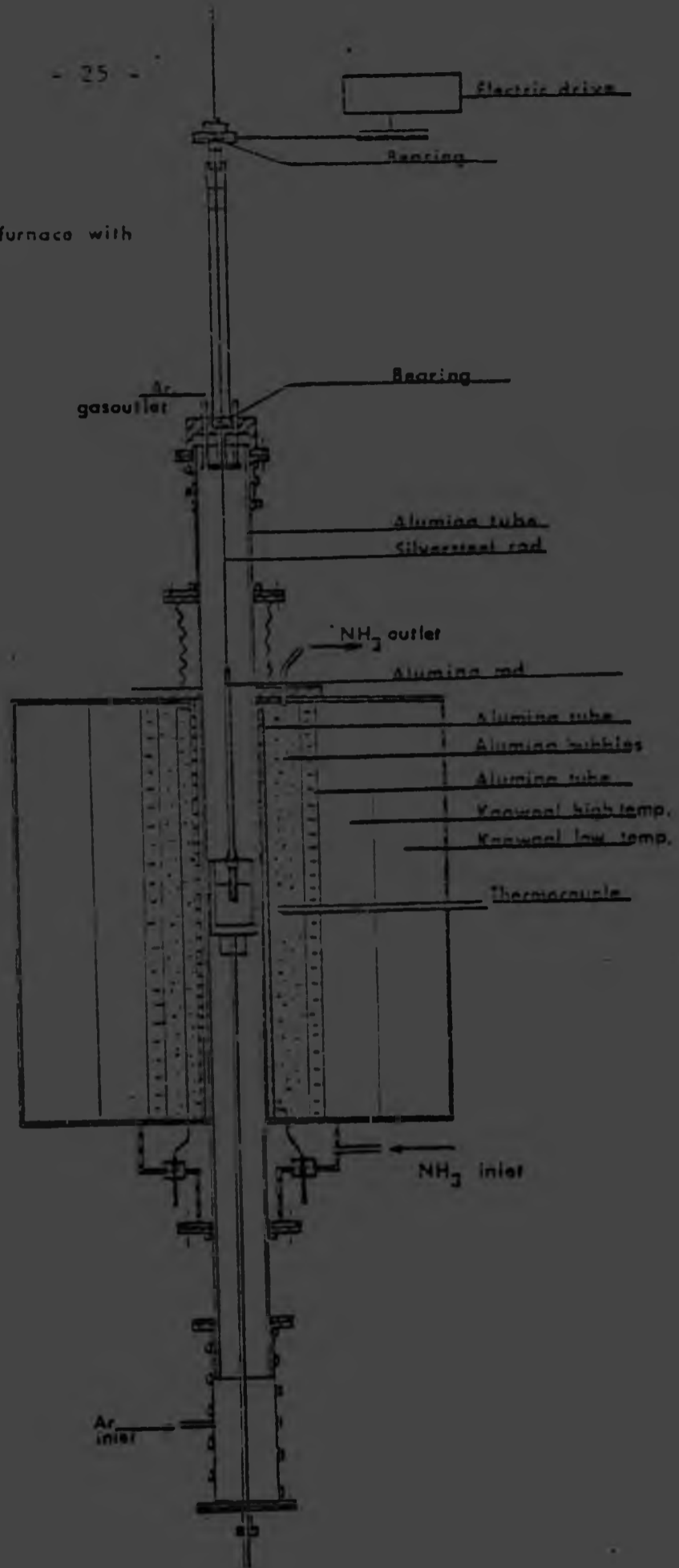
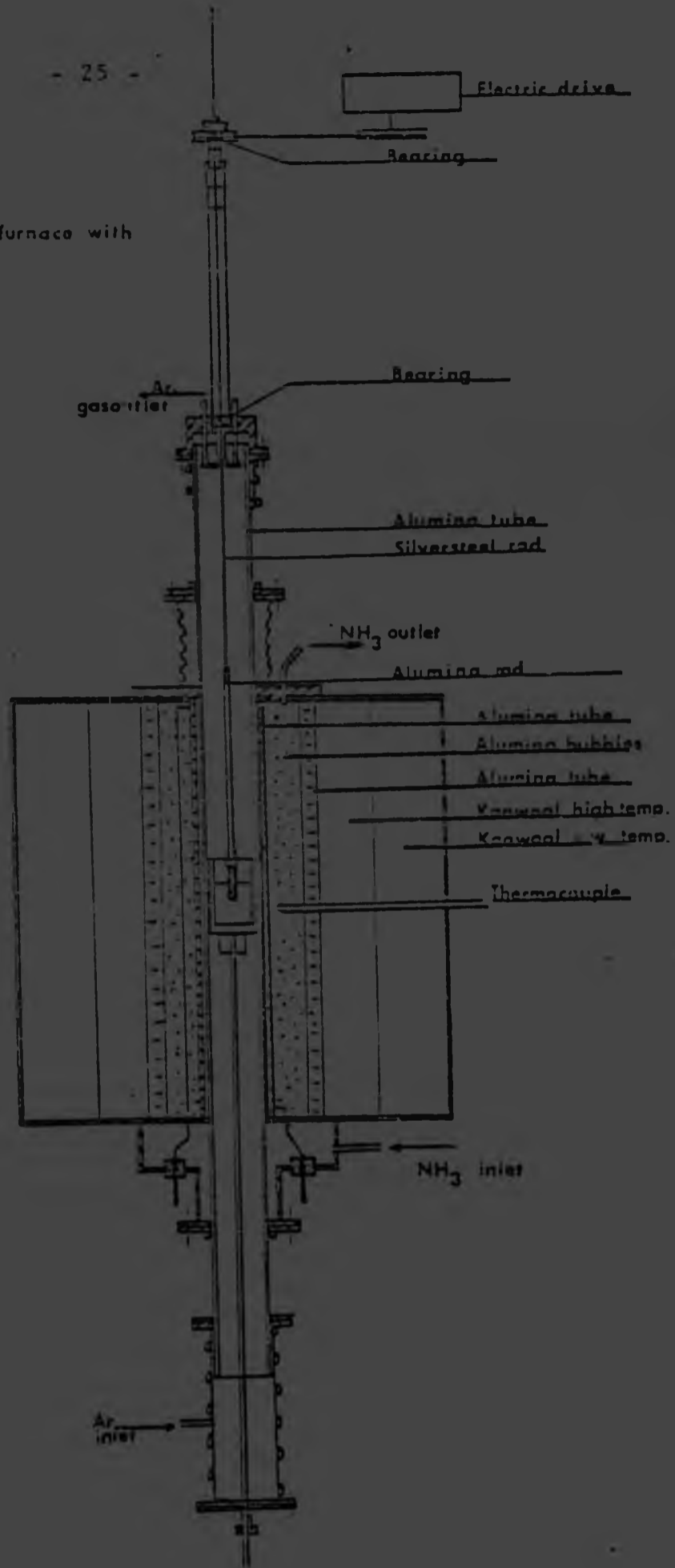


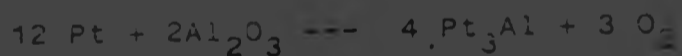
FIGURE 5.
Molybdenum wound furnace with
a rotating cylinder



the hot zone is monitored via a control thermocouple inserted from the side of the furnace with approximately 1,0 - 1,5 cm distance from the winding. A 6%Rh/Pt v. 30% Rh/Pt thermocouple is used for this purpose. The molybdenum wire has to be protected from oxidation at the high temperatures (1500 - 1700°C) at which the experiments are performed. For this purpose a constant stream of NH_3 is passed through the furnace at rates of 10-20 ml/min. At temperatures above 800°C the ammonia dissociates endothermically into hydrogen and nitrogen. Any oxygen leaking into the furnace area around the molybdenum winding will react with the hydrogen forming water vapour.

Unfortunately it appeared also that the hydrogen atmosphere has a deteriorating effect on the control thermocouple at the highest temperatures (1650-1750°C). The hydrogen diffuses through the alumina protection tube around the thermocouple. The following reaction takes place

Possibly



under influence of the strongly reducing H_2 atmosphere (33).

Several experiments had to be terminated because of this phenomenon.

During later runs the control thermocouple was bypassed and the thermocouple inside the tube was used as a control thermocouple as well as a thermocouple to measure the exact temperature of the crucible. Here no difficulties were encountered.

The atmosphere inside the tube is deoxygenized argon. Flowrate 10-20 ml/min. Before it is passed

into the furnace the argon (spectrographic grade) is led through concentrated sulphuric acid, to remove any hydrocarbons, next it is led over Ca Cl_2 , Mg ClO_4 and ascarite (soda-asbestos) to remove all traces of watervapour and CO_2 , finally it is led over copper chips at 500°C to remove all oxygen. The argon is passed into the bottom of the inner tube of the furnace via a PVC tube.

Unfortunately at a later stage, it was found that oxygen from the air diffused through the PVC tube into the argon thus causing some oxidation on the outside of the molybdenum crucible in the hot zone of the furnace. The oxides vapourize immediately and are deposited in cooler zones of the furnace. Nothing was done about it because it did not influence the experiments. At 1700°C in the molybdenum wound furnace numerous difficulties were encountered during the experiments, such as fuses burning out in the Eurotherm controller, furnace windings burning out and cracking of the inner tubes. Many experiments had to be terminated because of these reasons. It was decided therefore that for these temperatures and higher another furnace should be used.

An induction furnace was available with a watercooled gastight casing around the induction coil previously used for viscosity measurements of slags at high temperatures ($1600 - 1700^\circ\text{C}$) (34). The casing had to be adapted for a larger diameter alumina tube. The furnace head with the bearings could be fitted on the casing without much difficulty. About 10 test runs were performed with this setup. As a control thermocouple a Tungsten/Tungsten 26% Rhenium thermocouple was used because the 6%Rh/Pt v 30%Rh/Pt thermocouples are more or less at their upper limit at 1700°C .

All runs performed with this setup were very disappointing due to the following reasons:

- 1) Excessive oxidation of the molybdenum crucibles as well as of the W/26%Re thermocouple in spite of protective tubes (alumina). The obvious reason for this is leaks in the seals. In spite of many tries to improve this, there was no improvement.
- 2) Arcing between coil and casing and between the various turns of the coil thus causing the furnace electricity supply to trip out or causing leaks in the watercooled coil and filling the whole casing with water.

The induction furnace delivers a high frequency current of 500kHz. The coil induces a high frequency magnetic field which in its turn induces a high frequency current in the molybdenum crucible. The penetration depth of this field is very small so the current will flow only in the outer edge of the crucible. This means that the outside of the crucible has a considerable higher temperature than the inside and thus heats up the inside. Much heat is lost by radiation which prevents the achievement of high temperatures for the inside of the crucible + slag. The hot outside also enhances oxidation of the crucible surface filling the casing with molybdenum oxide vapours which can cause arcing in the coil.

A later modification of the system used graphite foil wound around the crucible (approximately 1 mm thick) as a susceptor. It was hoped that this would suppress excessive oxidation of the molybdenum and to give a better power coupling between coil and crucible.

This solution presented new problems though : the graphite reduced the recrystallized alumina tube, due to the fact that the graphite and the alumina tube were in contact with each other, the aluminium vapour thus causing similar problems as before (arcing). At this stage further experiments with this setup were considered not feasible. Also the need for these experiments at high temperatures (1700°C and higher) was not present anymore when it was found that the chromite cylinders fall apart at about 1720°C.

During these experiments the use of a pyrometer to measure the temperature has been tried out. During calibration it was obvious that this proved to be a failure. Fumes rising from the crucible made it impossible to measure the temperature with any degree of accuracy; differences up to 300°C were measured between the pyrometer reading and the thermocouple reading. The pyrometer readings were always lower.

3.3 Dissolution Experiments

The chromite cylinders were drilled from Winterveld ore lumps with a brass bonded 14 mm diamond core drill. Although many of the cylinders drilled this way were not suitable for the experiments, about 50% of the cores proved to be satisfactory i.e. smooth surface, no cracks, sufficient strength and sufficient length (minimum about 3,5 cm) Plate 1. The cylinder is connected to the alumina rod with an aluminium crucible (inside dia 16 mm) and high purity alumina cement. In a later version part of this cement was replaced by a sort of alumina glue (Haldenwanger type AB cement) which has a high strength at room



Small amount of material
for analysis of structure
of the material.

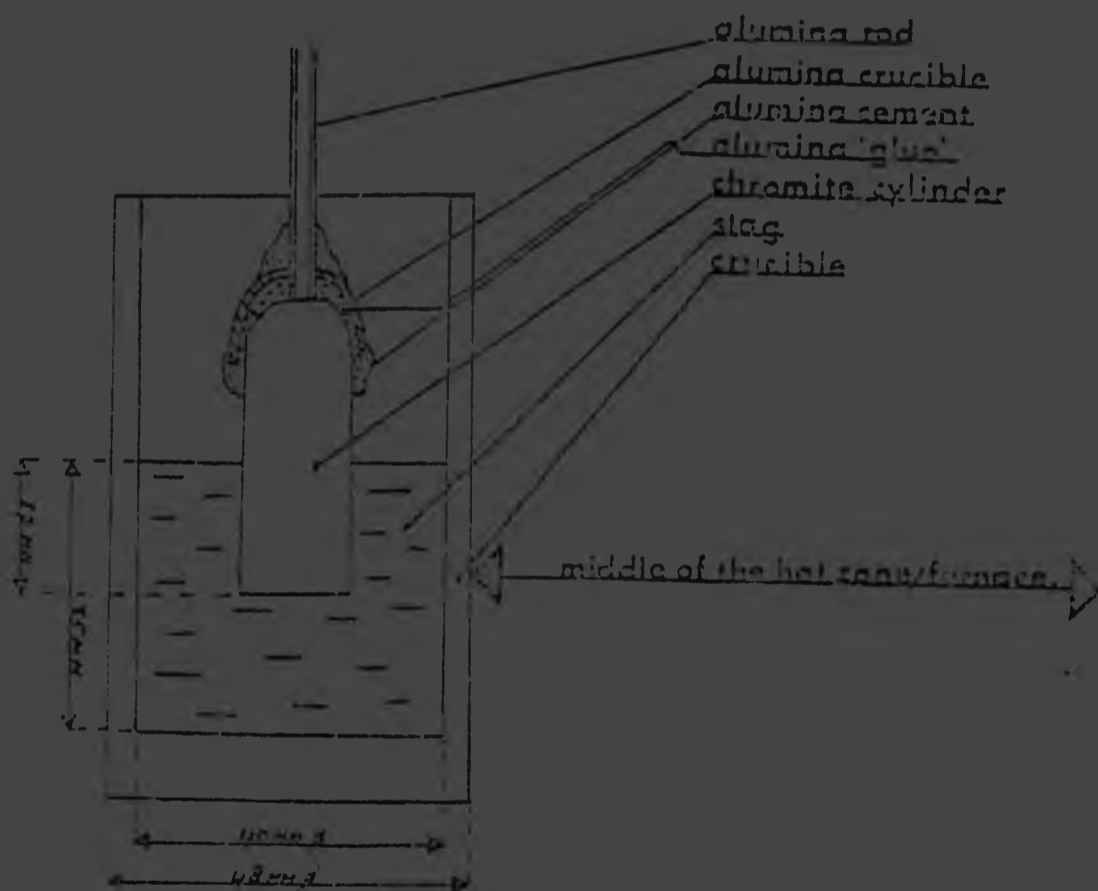
temperature up to about 1500°C (fig.6). The alumina rod, length approximately 15 - 20 cm, is connected with a silversteel rod (length 70 cm) with alumina cement. These connections proved to be strong enough during the experiments but needed careful handling at room temperatures because the alumina cement has virtually no 'green' strength. During the experiments the alumina rod showed the tendency to lose its straightness due to centrifugal forces at the high temperatures used.

Exact positioning of the cylinder with regard to the slag level also posed some problems. Prepositioning the crucible in the hot zone and the chromite cylinder at a certain level above it, then lowering the cylinder, when the whole system is at the required temperature, according to the set difference in level failed due to the thermal expansion of the rods. It was possible though to feel the slag level while lowering the cylinder into the slag by hand as a point of increased resistance to lowering. After the slag level had been felt, it was just a matter of marking the position on the rod and lowering the cylinder and rod to the required level. The accuracy of this method was about 1 mm.

After each run, the cylinders were examined and if possible their immersion depth was checked and compared with the setpoint. No deviations were measured on 2 cylinders. With all other cylinders the level could not be checked, because there was no change along the cylinder surface due to limited solution.

FIGURE 6.

MOLYBDENUM CRUCIBLE, SLAG AND ROTATING CYLINDER.



3.4 Optical microscope, microprobe and electron microscope

Some experiments with the rotating cylinder failed because the chromite cylinder broke during the experiment and dropped into the slag. Polished sections were made from the chromite cylinders and slag in order to investigate the dissolution effects more closely. Micrographs were taken of the reaction rim.

These sections were also investigated with an electron microscope and attached Edax system, which is able to analyse the x-rays emitted by the sample due to the electron bombardment. With this technique it is possible to make element distribution maps. These maps show relative concentrations of a certain element (plate 2-17).

More accurate measurements of the composition of the reaction rim and other areas were made by the electron microprobe. (table 11)

4 RESULTS

4.1 Quantitative Results

The quantitative results consist of the chemical analysis made of the slag samples as described in chapter 4.2. The results are presented in table 10 and figure 7.

Table 10. Chemical analysis of slag before and after dissolution experiments (mass percent).

TEMP. and TIME	Cr ₂ O ₃	FeO	SiO ₂	MgO	Al ₂ O ₃	CaO
pure slag	-	not measured	45,0	29,0	18,3	8,3
pure slag	-	0,35	45,3	29,2	18,0	8,5
1650°C 60 min.	<0,5	0,6	44,0	27,3	17,6	8,00
1650°C 120 min.	<0,5	0,75	42,5	27,1	18,5	7,65
1650°C 180 min.	<0,5	0,75	42,5	27,0	18,4	7,65
1650°C 180 min.	<0,5	0,9	42,1	26,3	18,4	7,65
1650°C 180 min.	<0,5	0,9	42,2	27,0	18,4	7,65
1600°C 60 min.	<0,5	0,55	44,8	26,0	18,1	8,25
1600°C 120 min.	<0,5	0,80	44,3	27,5	18,1	8,25
1600°C 120 min.	<0,5	0,80	44,3	27,5	18,1	8,25
1600°C 180 min.	<0,5	0,85	43,4	28,8	17,6	7,95
1550°C 60 min.	<1,0	0,5	44,0	31,1	17,9	8,3
1550°C 120 min.	<1,0	0,6	45,1	29,2	18,5	8,6
1550°C 180 min.	<1,0	0,7	40,2	27,0	22,2	7,3

4 RESULTS

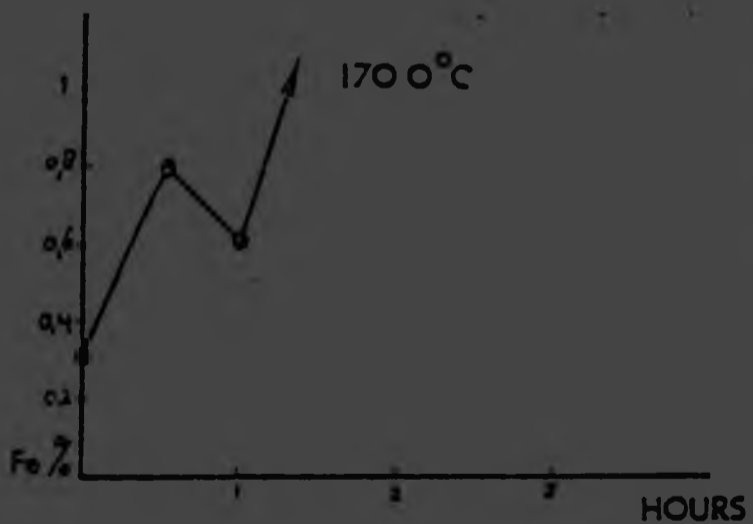
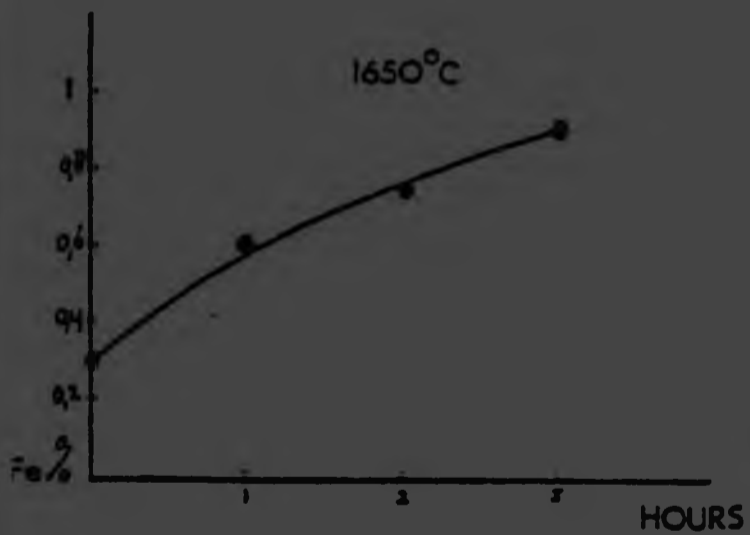
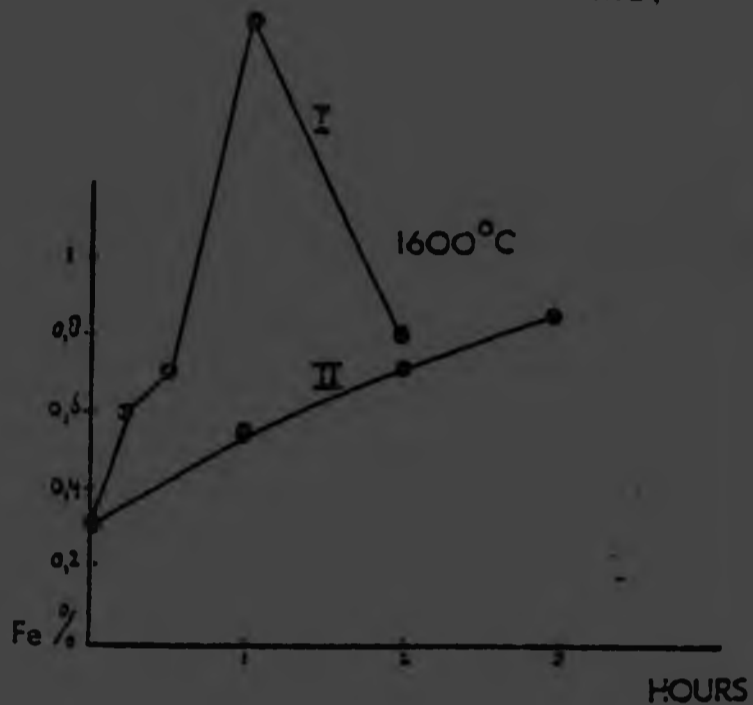
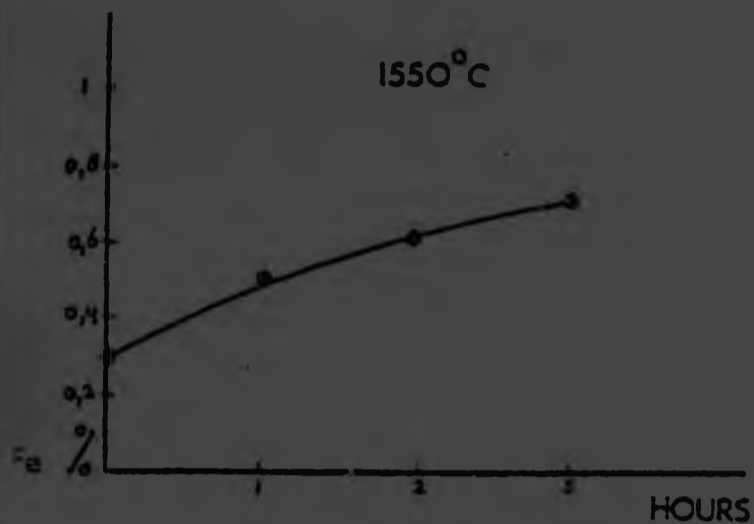
4.1 Quantitative Results

The quantitative results consist of the chemical analysis made of the slag samples as described in chapter 4.2. The results are presented in table 10 and figure 7.

Table 10. Chemical analysis of slag before and after dissolution experiments (mass percent).

TEMP. and TIME	Cr ₂ O ₃	FeO	SiO ₂	MgO	Al ₂ O ₃	CaO
pure slag	-	not measured	45,0	29,0	18,3	8,3
pure slag	-	0,35	45,3	29,2	18,0	8,5
1650°C 60 min.	<0,5	0,6	44,0	27,3	17,6	8,00
1650°C 120 min.	<0,5	0,75	42,5	27,1	18,5	7,65
	<0,5	0,75	42,5	27,0	18,4	7,65
1650°C 180 min.	<0,5	0,9	42,1	26,3	18,4	7,65
	<0,5	0,9	42,2	27,0	18,4	7,65
1600°C 60 min.	<0,5	0,55	44,8	28,0	18,1	8,25
1600°C 120 min.	<0,5	0,80	44,3	27,5	18,1	8,25
	<0,5	0,80	44,3	27,8	18,1	8,25
1600°C 180 min.	<0,5	0,85	43,4	28,8	17,6	7,95
1550°C 60 min.	<1,0	0,5	44,0	31,1	17,9	8,3
1550°C 120 min.	<1,0	0,6	45,1	29,2	18,5	8,6
1550°C 180 min.	<1,0	0,7	40,2	27,0	22,2	7,3

FIGURE 7. PERCENTAGE IRON DISSOLVED IN A SLAG PLOTTED AGAINST TIME, AT VARIOUS TEMPERATURES.



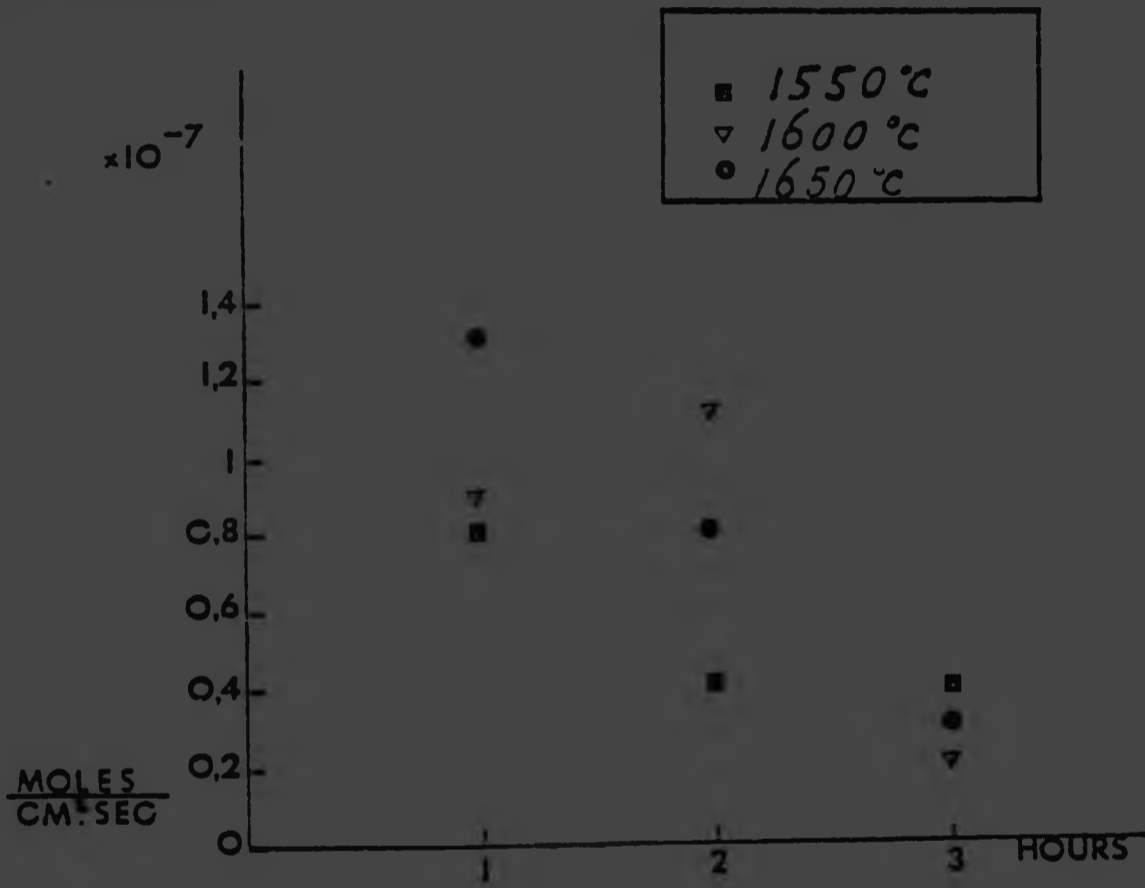
These results were used to calculate the average mass fluxes of iron from the cylinder to the slag (fig 8). The chromium analysis could not be used for this purpose as the concentrations of the chromium in the slag were below the sensitivity range of the method used to analyse the slag (induction coupled plasma spectrographic method). The average mass fluxes were calculated as shown in Appendix 1.

Several slag samples were analysed twice to check the accuracy of the analysis. Table 10 shows that the variation of the analysis for iron is very small. On the other hand, some variation occurs for other components especially for MgO. The relative variation is at the most 6.3% for MgO while for the other analysis values of 1% are typical.

Other quantitative results were obtained with the microprobe analysis of the chromite and the reaction rim (table 11). The analysis of column 1-4 are analysis of the bulk of the chromite. As can be expected, some variation exists between the results because the chromite is not constant in composition. The elements are more or less stochastically distributed in the spinel. The average composition of the chromite is shown in column 5.

The values for the reaction rim show some variation as well (columns 5-8) and the average is presented in column 9. These data are shown in the form of concentration profiles in fig 9. The size of the spot analysed with this technique is about 3-5 micron in diameter due to fluorescence and shifting of the electron beam compared to the reaction rim which has an average thickness of 30 μ n. As standards Stillwater chromite, rhodonite and Obergarden ilmenite are used.

FIGURE 8. RATES OF DISSOLUTION OF IRON-IONS, COMING FROM WINTERVELD CHROMITE, INTO A SLAG.



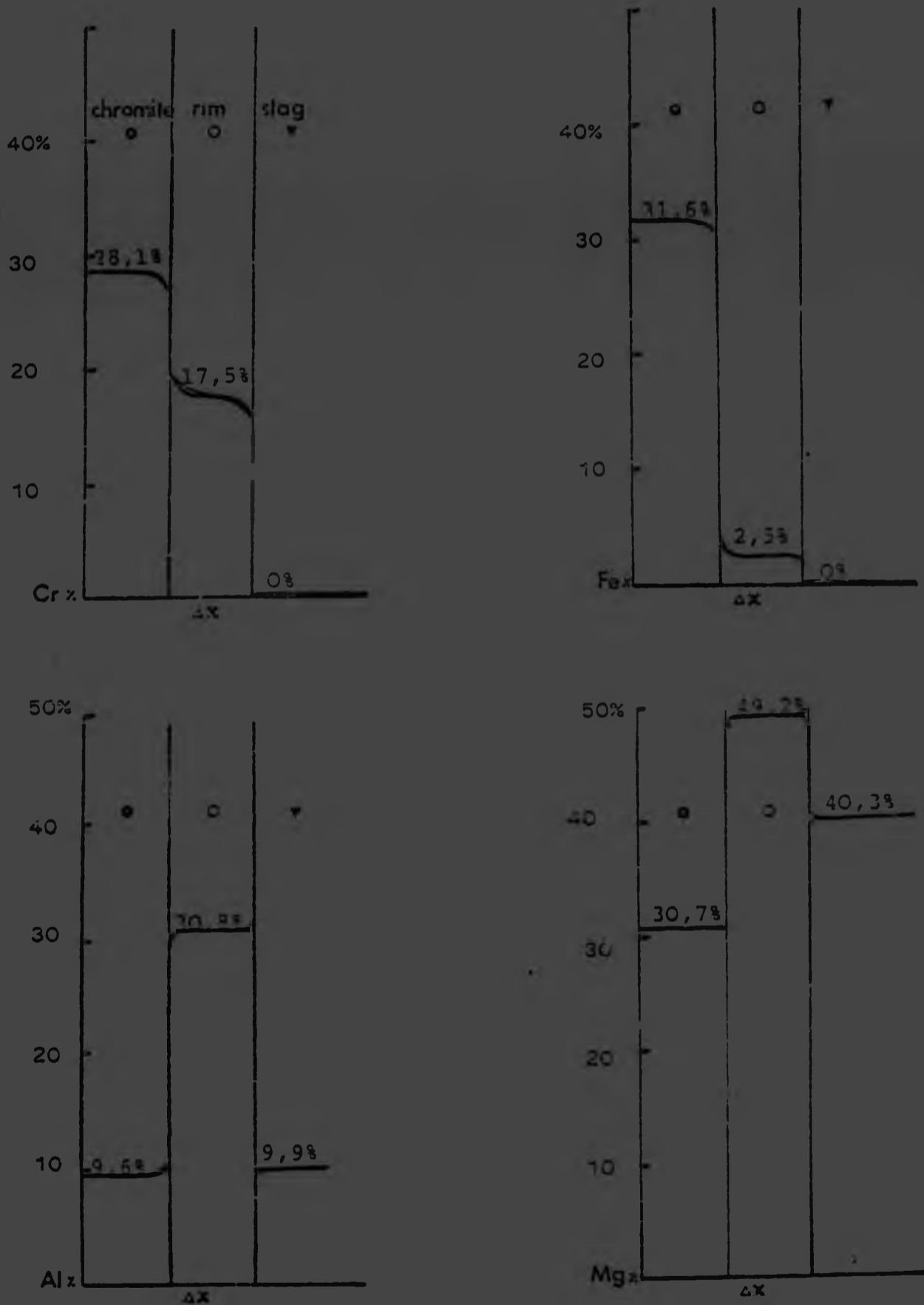


Figure 9 . Concentration profiles for Cr, Fe, Al and Mg over Chromite , reactionrim and slag. (in molepercentages)
 Δx = the average thickness of the reactionrim = 30 m^{-6} .

Table 11 - Electron microprobe analysis for the bulk of the chromite and the reaction rim (mass percentages)

	<u>1.</u>	<u>2.</u>	<u>3.</u>	<u>4.</u>	<u>5. average</u>	<u>6.</u>	<u>7.</u>	<u>8.</u>	<u>9. average</u>
SiO ₂	0,02	0,04	0,03	0,02	0,03	0,25	0,23	0,25	0,24
CaO	0	0	0	0,02	0,01	0,03	0,08	0,06	0,06
TiO ₂	0,84	0,84	0,87	0,82	0,84	0,03	0,05	0,01	0,03
Cr ₂ O ₃	47,95	48,41	47,98	48,37	48,18	32,62	32,06	31,16	31,95
FeO	25,78	25,60	24,98	22,43	24,70	1,36	1,9	1,82	1,69
MgO	10,86	10,72	11,02	12,57	11,29	23,96	23,64	23,49	23,70
Al ₂ O ₃	13,27	13,4	13,76	13,80	13,56	37,7	37,82	38,37	37,96
MnO	0,39	0,38	0,33	0,31	0,35	0,09	0,04	0,05	0,06
TOTAL	99,09%	99,39%	98,99%	98,37%	98,96%	96,03%	95,83%	95,22%	95,69%

Chromite 1 - 5

Reaction rim 6 - 9

Table 11 - Electron microprobe analysis for the bulk of the chromite and the reaction rim (mass percentages)

	<u>1.</u>	<u>2.</u>	<u>3.</u>	<u>4.</u>	<u>5.average</u>	<u>6.</u>	<u>7.</u>	<u>8.</u>	<u>9.average</u>
SiO ₂	0,02	0,04	0,03	0,02	0,03	0,25	0,23	0,25	0,24
CaO	0	0	0	0,02	0,01	0,03	0,08	0,06	0,06
TiO ₂	0,84	0,84	0,87	0,82	0,84	0,03	0,05	0,01	0,03
Cr ₂ O ₃	47,95	48,41	47,98	48,37	48,18	32,62	32,06	31,15	31,95
FeO	25,78	25,60	24,98	22,43	24,70	1,36	1,9	1,82	1,69
MgO	10,86	10,72	11,02	12,57	11,29	23,96	23,64	23,49	23,70
Al ₂ O ₃	13,27	13,4	13,76	13,80	13,55	37,7	37,82	38,37	37,96
MnO	0,39	0,38	0,33	0,31	0,35	0,09	0,04	0,05	0,06
TOTAL	99,09%	99,39%	98,99%	98,37%	98,96%	96,03%	95,83%	95,22%	95,69%

Chromite 1 - 5

Reaction rim 6 - 9

4.2 Qualitative Results

Polished sections were made of the chromite cylinders and slag. One cylinder had been for ½ hour at 1720°C while another had been for three hours at 1600°C. and one for three hours at 1550°C. These sections were investigated under an optical microscope. This investigation showed that the reaction rim is about 20-40 microns thick in all cases. It has in all cases the same porous structure (plate 2,3,4). At 1720°C the chromite seems to fall apart (plate 3) into its separate grains. This did not take place at lower temperatures where the cylinder after use always had a smooth surface with no grains missing on the surface. Some plates show a light phase in the slag and the reaction rim. This is not a metal phase but an unidentified silicate phase (plate 2,3,4). Pieces of the reaction rim detach and are transported into the slag as plates 2 and 3 show. Plate 4 shows the thin bands of gangue material between the chromite grains as well as how strongly the chromite grains are intergrown.

The pictures taken with the electron microscope and Edax system show the areas and the element distribution maps for iron, chromium, aluminium, magnesium and silicon (plates 5-17). Also some spot analysis were done with this apparatus on the chromite and the reaction rim. The accuracy of these measurements is very low and they are treated as qualitative results and are given in table 12 as ratios rather than absolute values.



Plate 2 - Chromite, reaction rim and slag
30 minutes at 1650°C |-----| = 50m
● chromite
★ Reaction rim
☆ Slag crystallisation products
○ unidentified silicate phase



Plate 3 - Chromite, reaction rim and slag
10 minutes at 1720°C |-----| = 100m
● chromite
★ Slag
★ Reaction rim
○ Slag crystallisation products
○ Piece of the Reaction rim.



● Chromite
● Magnetite

Scale bar
100 m



- ☆ Slag
- * Reaction rim
- * Chromite

Plate 5 - Electronmicrograph of chromite
reaction rim and slag, 1 hr at 1600°C

— 1000 Å

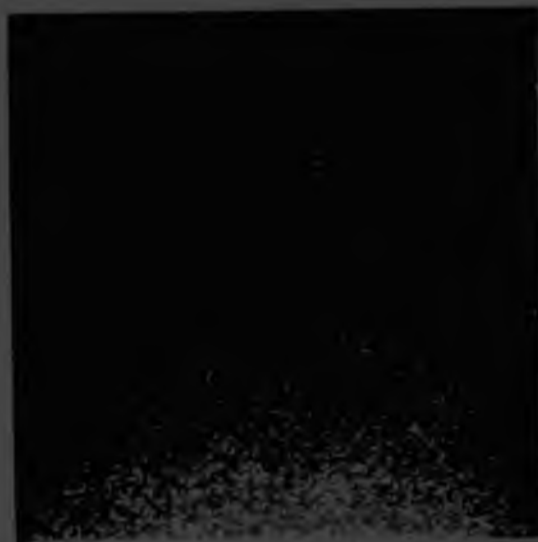


Plate 8
Distribution of
Aluminum

Plate 9
Distribution of
Magnesium



Distribution of Chromium



Iron



Plate 8
Distribution of
Aluminium

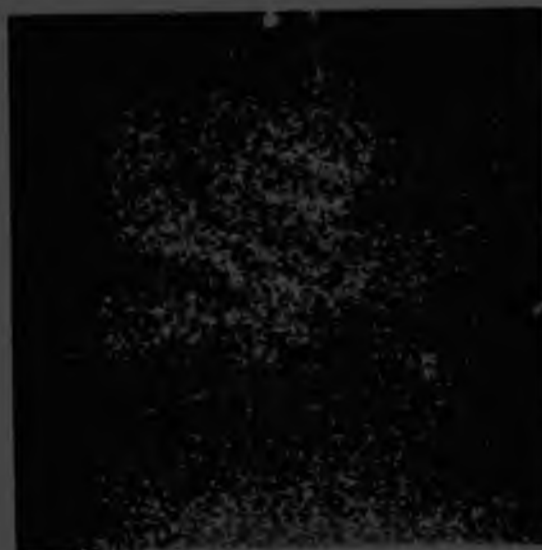


Plate 9
Distribution of
Magnesium



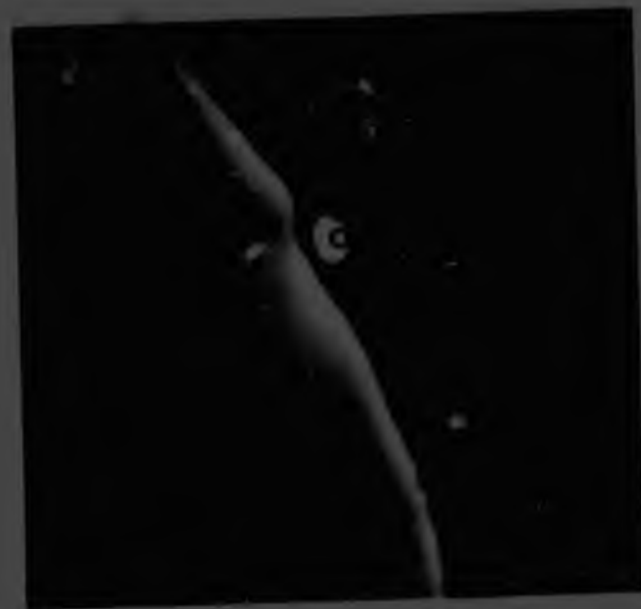
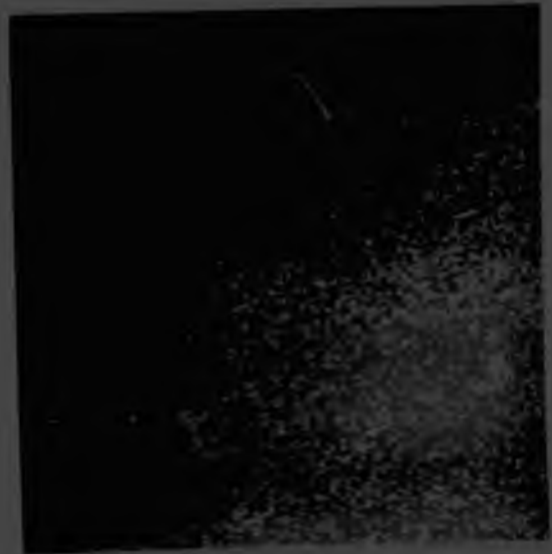
- Slag
- Reaction rim
- ◆ Chromite

Plate 10- Electronmicrograph of chromite and the reaction rim, 1 hr at 1600°C

— 10⁻⁶ —



Plate 11 - Distribution of chromium



- Sideromorphite
- chromite
- gangue mineral

Plate 14 - Chromite with a gangue mineral.
1 hr at 1600°C

— = 5m⁻⁶



Plate 15 - Distribution of Chromium



Plate 16 -
Distribution of Magnesium

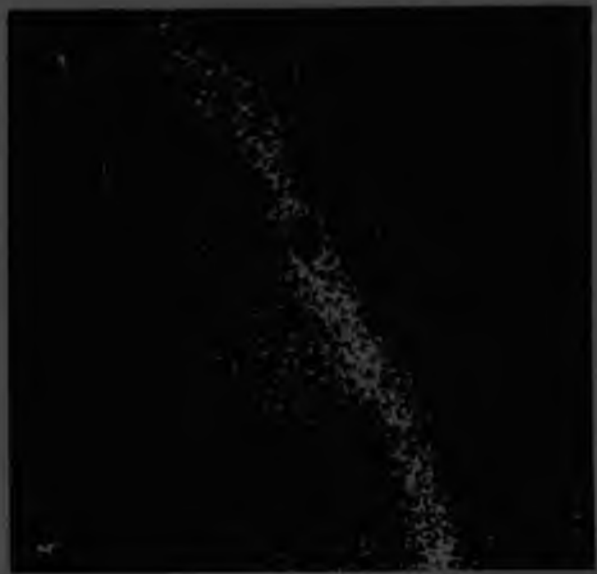


Plate 17 -
Distribution of Silicon

Table 12 - Spot analysis done with the Edax

The ratio for various oxides of the bulk of the chromite and the reaction rim.

Cr_2O_3	ratio chromite/reaction rim	3,5
FeO	" " " "	14,6
Al_2O_3	" " " "	0,43
MgO	" " " "	0,75

The reaction rim which was observed in all polished sections is a thin differently coloured layer between the slag and the chromite. This rim has formed due to the interaction of slag and chromite at high temperatures.

5 DISCUSSION

The writer feels that the performance of the rotating cylinder technique at high temperatures is satisfactory in the sense that it gives meaningful data of the rate of dissolution.

The setup needs more development though, in order to overcome the eccentricity that develops in the rotating part during the experiments. Then the mass transfer correlations applicable to this system can be truly applied and used to obtain data about diffusion coefficients, mass transfer coefficients and reaction rates of the system chromite-slag. The eccentricity of the rotating part develops due to the centrifugal forces exerted on the rod during rotation at high temperatures.

The fact also that the rotating part consists of three separate elements (chromite cylinder, alumina rod and silversteel rod) which have to be aligned very carefully, contribute to any existing eccentricity. The experiments were performed at only one speed, 44 rpm, which was about the slowest speed obtainable. The reason for doing runs at only one speed was that at higher speeds slag was spilled out of the crucible due to the eccentricity of the chromite cylinder. The peripheral speed of the cylinder at 44 rpm is as such too slow to induce a turbulent regime in the slag if the cylinder was perfectly centered. This is demonstrated by the Reynolds number at the different temperatures.

$$\text{Re} = \frac{u \cdot l}{\nu} \quad (13) \quad \begin{array}{l} u = 3,21 \text{ cm/sec} \quad (44 \text{ rpm}) \\ l = 1,4 \text{ cm} \end{array}$$

Results :	1550°C	v = 1,34 stokes (cm ² /sec)	Re = 3,4
	1600°C	v = 1,02 "	Re = 4,4
	1650°C	v = 0,78 "	Re = 5,8
	1700°C	v = 0,60 "	Re = 7,5

$\nu = \frac{\eta}{\rho}$. (6) The values for η are as discussed in paragraph 3.3 while the value for ρ was obtained experimentally.

These values for the Reynolds number are in the laminar region. If we assume an eccentricity during the experiment of 0,5 cm we get Re-values between 15-35, which is in turbulent region (9) whereby l is taken as $1,4 + 0,5 + 0,5 = 2,4$ cm and $u = 2 \cdot \pi \cdot 1,9 \times 10^{-4} / 60 = 8,75$

The turbulence is caused by temperature differences between top and bottom of the crucible (at 1250°C about 10°C) (fig 10) as well as between the wall of the crucible and the middle of the system. Although these temperature profiles were taken at lower temperatures they show that some temperature difference occurs between bottom and top. The slags that were taken out of the crucible after slow cooling were always uniform in colour and in texture.

This uniformity indicates that the slag is completely mixed so turbulent conditions existed during the dissolution process. As discussed in 4.1 the accuracy of the results is good.

Because the slag does not show any detectable increase in chromium levels, the chromium levels as shown in table 10 are not suitable to investigate the dissolution rate of the chromite. Therefore the data for iron were used (fig 7). Average mass fluxes were calculated for the 1st, 2nd and 3rd hour of the experiments (fig 8 and table 13).

FIGURE 10 - TEMPERATURE PROFILE OF A MOLYBDENUM WOUND FURNACE.

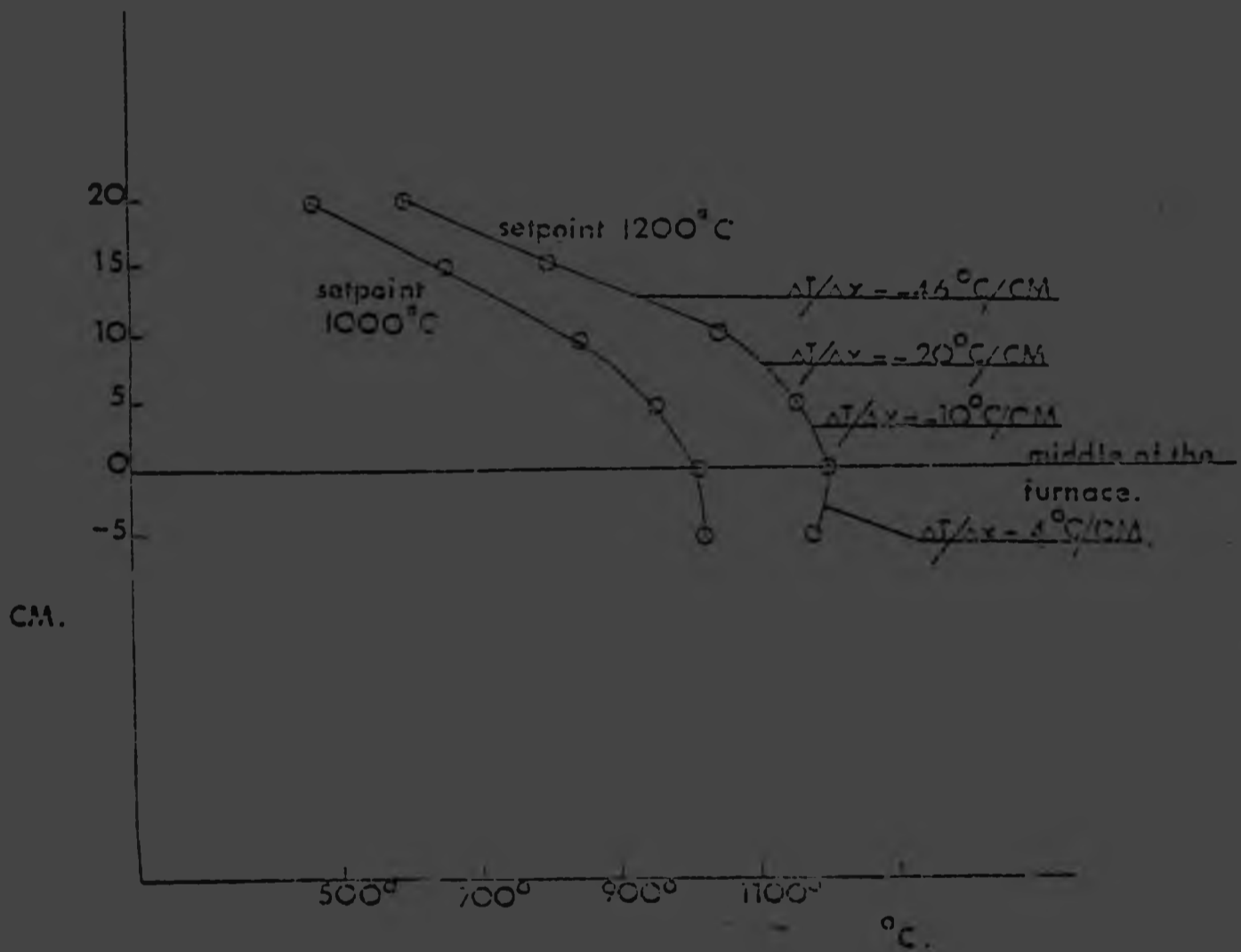


Table 13 - Average mass fluxes of iron ions from the chromite cylinder to the slag.

(moles/cm ² /sec.)	1550°C	1600°C	1650°C
1st hour	$0,8 \times 10^{-7}$	$0,9 \times 10^{-7}$	$1,3 \times 10^{-7}$
2nd hour	$0,4 \times 10^{-7}$	$1,1 \times 10^{-7}$	$0,8 \times 10^{-7}$
3rd hour	$0,4 \times 10^{-7}$	$0,2 \times 10^{-7}$	$0,3 \times 10^{-7}$

Fig 8 shows that the average massflux has the tendency to decrease with time.

In appendix 3 a calculation is shown using the mass transfer correlation for a rotating cylinder. For a large variety of circumstances the mass transfer coefficient k was calculated for the range of T between 1550°C - 1700°C and a viscosity range of 1,34 - 0,6 stokes. For the peripheral speed, the range 44 - 4400 rpm was used to allow for the eccentricity. The diffusion coefficients as described in paragraph 2.2.2 were used ranging from 7×10^{-6} to $1,4 \times 10^{-5}$ cm²/sec. Thus we obtain the matrix for k table 14.

Table 14 $k = 0,079 \cdot Re^{-0,3} \cdot Sc^{-0,644}$ for different values of peripheral speed and temperature.

	44 rpm	440 rpm	660 rpm	4400 rpm
1550°C	$0,04 \cdot 10^{-3}$	$0,27 \cdot 10^{-3}$	$0,39 \cdot 10^{-3}$	$1,03 \cdot 10^{-3}$
1600°C	$0,05 \cdot 10^{-3}$	$0,46 \cdot 10^{-3}$	$0,68 \cdot 10^{-3}$	$1,70 \cdot 10^{-3}$
1650°C	$0,1 \cdot 10^{-3}$	$0,76 \cdot 10^{-3}$	$1,14 \cdot 10^{-3}$	$2,83 \cdot 10^{-3}$
1700°C	$0,16 \cdot 10^{-3}$	$1,18 \cdot 10^{-3}$	$1,66 \cdot 10^{-3}$	$4,36 \cdot 10^{-3}$

If Reynolds numbers are taken in the region 15 - 35 results shown in table 15 are obtained.

Table 15 - Different values for Reynolds number and the mass transfer coefficient (k) for various temperatures.

	Re	k
1550°C	Re = 15,7	$0,08 \cdot 10^{-3}$
1600°C	Re = 20,6	$0,16 \cdot 10^{-3}$
1650°C	Re = 26,9	$0,24 \cdot 10^{-3}$
1700°C	Re = 35	$0,36 \cdot 10^{-3}$

For the total mass flux the following formula (12) was used.

$$n = k (C_s - C_b) \quad (12)$$

$$J = \dot{n} \cdot A \quad (17) \text{ moles/sec total flux}$$

$$A = \text{area cylinder cm}^2$$

For the concentration of the bulk of the slag (C_b) an average concentration is taken. $C_{b(ave)}$ is calculated by taking a concentration halfway between the starting and the finishing concentration.

The concentration of the iron in the chromite posed a problem. The dissolution mechanism is not fully understood and the formation of the 'inert' layer on the chromite of which the average composition during the dissolution process is not known. So some values were assumed of C_s between the chromite composition and the reaction rim composition as measured (table 16).

Table 12 - Concentration gradients over the interface chromite-slag for various percentages of FeO in the chromite and the mass fluxes as result of the gradients.

A = 6,6 cm ²	$\Delta C \times 10^{14}$			K x 10 ⁺³	J		
	1st hr	2nd hr	3rd hr		1st hr	2nd hr	3rd hr
1550°C							
FeO 20%	120,4	119,9	119,5)	0,08	$6,36 \cdot 10^{-6}$	$6,33 \cdot 10^{-6}$	$6,31 \cdot 10^{-6}$
15%	85,7	85,2	84,8)		$4,53 \cdot 10^{-6}$	$4,50 \cdot 10^{-6}$	$4,48 \cdot 10^{-6}$
10%	53,8	53,3	52,9)		$2,89 \cdot 10^{-6}$	$2,81 \cdot 10^{-6}$	$2,79 \cdot 10^{-6}$
5%	24,6	24,1	23,7)		$1,30 \cdot 10^{-6}$	$1,27 \cdot 10^{-6}$	$1,25 \cdot 10^{-6}$
2%	8,2	7,7	7,3)		$0,43 \cdot 10^{-6}$	$0,41 \cdot 10^{-6}$	$0,39 \cdot 10^{-6}$
1500°C							
FeO 20%	120,3	119,4	118,7)	0,14	$11,12 \cdot 10^{-6}$	$11,03 \cdot 10^{-6}$	$10,97 \cdot 10^{-6}$
15%	85,6	84,7	84)		$7,91 \cdot 10^{-6}$	$7,83 \cdot 10^{-6}$	$7,76 \cdot 10^{-6}$
10%	53,7	52,8	52,1)		$4,96 \cdot 10^{-6}$	$4,88 \cdot 10^{-6}$	$4,81 \cdot 10^{-6}$
5%	24,5	23,6	22,9)		$2,26 \cdot 10^{-6}$	$2,18 \cdot 10^{-6}$	$2,12 \cdot 10^{-6}$
2%	8,1	7,2	6,5)		$0,75 \cdot 10^{-6}$	$0,67 \cdot 10^{-6}$	$0,60 \cdot 10^{-6}$
1650°C							
FeO 20%	120,2	119,4	118,7)	0,24	$19,04 \cdot 10^{-6}$	$18,91 \cdot 10^{-6}$	$18,80 \cdot 10^{-6}$
15%	85,5	84,7	84)		$13,54 \cdot 10^{-6}$	$13,43 \cdot 10^{-6}$	$13,31 \cdot 10^{-6}$
10%	53,6	52,8	52,1)		$8,49 \cdot 10^{-6}$	$8,36 \cdot 10^{-6}$	$8,25 \cdot 10^{-6}$
5%	24,4	23,6	22,9)		$3,87 \cdot 10^{-6}$	$3,74 \cdot 10^{-6}$	$3,63 \cdot 10^{-6}$
2%	8,0	7,2	6,2)		$1,27 \cdot 10^{-6}$	$1,14 \cdot 10^{-6}$	$0,98 \cdot 10^{-6}$

ΔC = Concentration difference between the reaction rim and the slag.

Table 16 - density weight perc. FeO mole/cm³ FeO
gr/cm³

chromite	4,4	24,7%	0,01509
reaction rim	3,6	1,7%	0,00125
value 1	4,4	20%	0,01222
value 2	4,2	15%	0,00875
value 3	4,0	10%	0,00556
value 4	3,8	5%	0,00264
value 5	3,6	2,0%	0,00100

Iron and chromium diffuse out of the spinel and are replaced by lighter elements, Al and Mg, thus the reaction rim will have a substantial lower density than chromite (estimated on 3,6 gr/cm³). (13).

With the electron microscope, some values were obtained for the reaction rim (table 11). It is not known whether these values represent end concentrations or concentrations somewhere during the leaching process.

Table 17 - Average composition of the slag during the various experiments in weight percent FeO and in mole/cm³.

	1st Hour	2nd Hour	3rd Hour
1550°C	0,41% $1,8 \cdot 10^{-4}$	0,55% $3,3 \cdot 10^{-4}$	0,65% $2,7 \cdot 10^{-4}$
1600°C	0,45% $1,9 \cdot 10^{-4}$	0,65% $2,8 \cdot 10^{-4}$	0,83% $3,5 \cdot 10^{-4}$
1650°C	0,48% $2 \cdot 10^{-4}$	0,68% $2,8 \cdot 10^{-4}$	0,83% $3,5 \cdot 10^{-4}$

Together with the formulas 17 and 12 and the data obtained in tables 15, 16 and 17 we get table 18:-

Comparing the results obtained in Table 18 with the results obtained by the dissolution experiments as shown in Table 13 and after multiplying them with the surface area of the cylinder ($6,6 \text{ cm}^2$) it is seen that the mass transfer rates are about the same magnitude as the experimental values if we assume an iron content of about 2% FeO (composition of the reaction rim) in contact with the slag.

Pictures taken of the chromite slag interface reveal the presence of a reaction layer of about 30 microns thick. (Plates 2,3) The interface chromite reaction rim is very sharp and straight in spite of the irregular shaped reaction rim allowing the slag to penetrate deep into the reaction rim close to the reaction interface. The composition of the reaction rim seems to be constant throughout the rim as several spot analysis taken with the microprobe show (Table 11). The sharp drop in the concentration of FeO and Cr_2O_3 when going from the chromite to the reaction rim indicates a change in phase. The process taking place at the interface is probably a diffusion controlled process with a moving interface i.e. the interface moves into a chromite.

Some calculations done on the diffusion in the chromite show that the magnitude of the mass flux due to diffusion is about the same as the experimentally measured mass fluxes. Formula 18 is used to calculate the mass fluxes. Several values for the thickness of the reaction rim were used.

$$\dot{n} = \frac{D \cdot \Delta C}{F} \quad (18) \quad \Delta C = 13,34 \cdot 10^{-3} \text{ moles/cm}^3$$

$$F_1 = 10 \cdot 10^{-3} \text{ cm}$$

$$F_2 = 20 \cdot 10^{-3} \text{ cm}$$

$$F_3 = 30 \cdot 10^{-3} \text{ cm}$$

The values for the diffusion coefficient in chromite in Table 2 were used and the difference in concentration of FeO in the chromite and the reaction rim from Table 11. The results of this calculation are shown in Table 19.

Table 19 - Mass fluxes of Fe due to diffusion at various temperatures and reaction rim thicknesses.

\dot{n} (moles/cm²/sec)

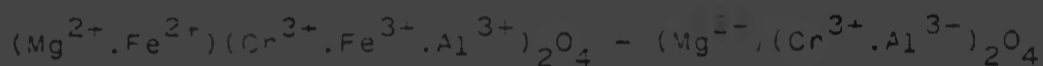
	F_1	F_2	F_3
1550°C	$0,1 \cdot 10^{-7}$	$0,05 \cdot 10^{-7}$	$0,03 \cdot 10^{-7}$
1600°C	$0,18 \cdot 10^{-7}$	$0,09 \cdot 10^{-7}$	$0,06 \cdot 10^{-7}$
1650°C	$0,32 \cdot 10^{-7}$	$0,17 \cdot 10^{-7}$	$0,11 \cdot 10^{-7}$

Comparing these values with the experimentally obtained values for the mass fluxes (table 13), it is clear that the dissolution process is not totally diffusion controlled. Other factors play a role in the dissolution mechanism as well. Higher measured values of FeO in the slag can be also caused by pieces of the reaction rim that break off and are transported into the slag (plates 2,3).

The change that seems to take place during the conversion chromite - reaction rim and which causes the slag to penetrate deeply into the reaction rim also

causes pieces to break off and determines how much of each oxide goes in or out of the reaction rim (appendix 4). This is quite important in the case of magnesia; If one assumes 1 mole of chromite is converted to an amount of x mole reaction rim then for $x > 0,62$ mole magnesia has to diffuse into the reaction rim while if $x < 0,62$ mole magnesia has to diffuse out. Cr_2O_3 and FeO will in every case diffuse out while Al_2O_3 diffuses in. An exact determination of the conversion process was not possible as shown in appendix 5, due to the variances in the slag analysis and since it is not known how much chromite is converted to reaction rim composition.

The analysis of the microprobe on the reaction rim indicate that a new spinel is formed.



The iron is preferentially leached out of the chromite into the slag. This is possibly because Fe^{3+} can get reduced to Fe^{2+} due to the low oxygen pressure in the system. This low oxygen pressure is reached due to the presence of Mo (molybdenum crucible) which has at these temperatures an equilibrium pressure of about 10^{-15} atm (P_{O_2}) in equilibrium with MoO_2 . Once the Fe is reduced to Fe^{2+} it gains a higher mobility as discussed in paragraph 2.1.2. Some of the Cr_2O_3 is leached out of the chromite as well. It is not clear though whether this happens as Cr^{3+} or as Cr^{2+} .

The element distribution maps (plates 3-16) show clearly the reaction rim which is depleted in Cr and Fe and enriched in Mg and Al. The other slag constituents

do not seem to play a role in the dissolution process except that SiO_2 serves as a solvent for the solutes as well as for MgO and Al_2O_3 .

Al_2O_3 can form only a very limited solid solution with chromite spinel. It is therefore probable that Al_2O_3 is part of the spinel in the reaction rim as MgAl_2O_4 or FeAl_2O_4 .

Besides this chemical leaching process, some other phenomena take place as observed in the microscope pictures (Plates 2,3). Pieces of the reaction rim break off due to viscous drag forces exerted on the rim by the slag during rotation of the cylinder. The pieces thus transported into the slag disturb, of course, the exactness of the chemical analysis because this measures the sum of both effects. This phenomena does not take place very frequently in the system. These pieces were very rare in the polished sections investigated or could not be found at all. The calculations on diffusion in the chromite (Table 19) show that the mass fluxes are not much higher than could be caused by diffusion. Under rougher circumstances, for instance when the slag is in highly turbulent conditions and the chromite grains rub against each other, it is possible that this effect contributes more to the dissolution process due to two factors:

- (a) Fresh chromite surfaces become available to chemical attack;
- (b) The reaction rim pieces present in the slag would enhance the chromium content of the slag as measured by the chemical analysis.

At a temperature of about 1700°C the chromite cylinder starts to fall apart into its separate grains, thus preventing any measurements with the rotating cylinder method. This effect can of course take place at lower temperatures if the forces on the chromite are large enough (viscous drag forces).

The gangue material as investigated in earlier works (18, 19) and shown in plates 4, 14 - 17 is probably a clinostatite which has a melting point of about 1550°C . This low melting point contradicts the fact that the chromite cylinder falls apart only at about 1700°C . Plate 4 shows that the chromite grains are very much intergrown so they could hold together even if the gangue material was fluid because it is present in such small veins and the grains cannot detach easily from each other without applying forces.

6. CONCLUSIONS

Three effects are responsible for the Cr and Fe content in the slag:

- 1) Chemical dissolution;
- 2) Mechanical action causing the reaction rim to break into pieces which are transported into the slag. By exposing fresh chromite surfaces to the slag it enhances effect 1;
- 3) Mechanical action causing the chromite cylinder to fall apart in its separate grains. The total surface area of the chromite is thus much larger and therefore effects 1 and 2 are increased.

Iron and chromium ions diffuse out of the chromite but the percentage chromium diffusing out is small compared with the iron.

Simultaneously aluminium and probably also magnesium diffuse into the spinel structure depleted of iron and chromium.

Magnesia and alumina probably exert an adverse effect on the dissolution rates.

The turbulent conditions which exist in the slag layer of a ferrochromium furnace enhance the dissolution of the chromite considerably. Due to the fact that the particles rub against each other, break off reaction rim pieces and thus expose unaltered chromite to the slag.

APPENDIX ONE

Example of a calculation of the average mass fluxes from the experimental data (slag analysis).

Starting composition slag 0,35 weight % FeO

after one hour at 1550°C 0,5 weight % FeO

FeO = 0,15 weight %, weight slag 110 gram

FeO = 0,165 grams molec. weight FeO = 72gr/mole

FeO = 0,002292 mole.

So the total flux during one hour is $\frac{0,002292}{3600} =$

$6,37 \cdot 10^{-7}$ mole/sec divided by the area of the cylinder ($6,6 \text{ cm}^2$) gives us $0,96 \cdot 10^{-7}$ mole/cm²/sec.

Taking the bottom area of the cylinder as well

$A = 8,14 \text{ cm}^2$ and the flux is $0,78 \cdot 10^{-7}$ mole/cm²/sec.

All values in Table 13 are for the total area of the cylinder.

APPENDIX TWO

Sensitivity analysis of the change of composition of the slag after refilling the slag mass with fresh slag.

Say there is 110 grams of slag in the crucible before sampling.

Concentration FeO = 0,6% (weight)

In crucible $110 \times 0,6/100 = 0,66$ gr FeO.

Assume a sample of 5 grams is taken.

The amount of FeO taken out of the crucible is

$$\frac{5 \times 0,6}{100} = 0,03 \text{ gr. and left in the slag is } 0,66 -$$

$$0,03 = 0,63 \text{ grams.}$$

Slag is refilled to original weight 110 grams.

$$\frac{0,63}{110} \times 100 = 0,573 \% \text{ FeO in slag.}$$

This change of the slag composition falls within the experimental error and can be disregarded.

APPENDIX THREE

The formula of the mass transfer coefficient can be expressed as

$$K = 0,079 \cdot \text{Re}^{-0,3} \cdot \text{Sc}^{-0,644} \cdot U \quad (\text{for rotating cylinder})$$

$$\text{Re} = \frac{U \cdot l}{\nu}$$

U = peripheral speed cylinder cm/sec
l = diameter cylinder cm
 ν = kinematic viscosity cm²/sec

$$\text{Sc} = \frac{\nu}{D}$$

D = diffusion coefficient cm²/sec

In the calculation of the kinematic viscosity the values obtained by Ossin (24) are used-

	1550°C	n = 4,03 poises	ν = 1,37 stokes
	1600°C	n = 3,05 poises	ν = 1,02 stokes
ν :	1650°C	n = 2,35 poises	ν = 0,78 stokes
	1700°C	n = 1,8 poises	ν = 0,6 stokes

Over the whole temperature range a density $\rho = 3,0$ gr/cm³ is used. At room temperature the density is 3,4 gr/cm³. This value was measured at 1600°C by 'feeling' the slag level in the crucible.

For various reasons it was not necessary to correct this density for higher or lower temperatures. The system is not behaving ideally so these calculations can only approximate the actual situation. The viscosities are not accurate either as the large differences between the measurements of several authors show. (1, 2, 3, 24)

The Reynolds and Schmidt numbers are calculated for a wide range of conditions and thus take into account any inaccuracy in the data used. "l" equaled 1,4 cm except at 1700°C where a change in the diameter was

observed of D_1 to be 1,3 cm diameter after two hours.
At all other temperatures the diameter of the cylinder
stayed constant.

The peripheral speed was during the experiments constant
3,21 cm/sec (44±2 rpm). In these calculations a wide
range of different speeds is taken to allow for the
non-idealities in the system.

- A) $u = 3,21$ cm/sec 44 rpm
- B) $u = 32,1$ cm/sec 440 rpm
- C) $u = 64,1$ cm/sec 660 rpm
- D) $u = 321$ cm/sec 4400 rpm

These give:-

$$\begin{aligned} Re_{1550} &= 3,35 \\ Re_{1600} &= 4,41 \\ Re_{1650} &= 5,76 \\ Re_{1700} &= 7,49 \end{aligned}$$

$$\begin{aligned} B) \quad Re_{1550} &= 33,5 \\ Re_{1600} &= 44,1 \\ Re_{1650} &= 57,6 \\ Re_{1700} &= 74,9 \end{aligned}$$

$$\begin{aligned} Re_{1550} &= 67 \\ Re_{1600} &= 88,2 \\ Re_{1650} &= 115,2 \\ Re_{1700} &= 149,8 \end{aligned}$$

$$\begin{aligned} D) \quad Re_{1550} &= 335 \\ Re_{1600} &= 441 \\ Re_{1650} &= 576 \\ Re_{1700} &= 749 \end{aligned}$$

The following diffusion coefficients are used as
discussed in chapter 2.2.2 (Table 7):

D_{Ca}	7×10^{-6}	1550°C
D	3×10^{-6}	1600°C
D	10^{-6}	1650°C
D	10^{-5}	1700°C

Together with the viscosity data I obtained the following values for the Schmidt numbers ($Sc = \frac{\mu}{D}$):

$$Sc_{1550} = 335 \cdot 10^3$$

$$Sc_{1660} = 128 \cdot 10^3$$

$$Sc_{1650} = 52 \cdot 10^3$$

$$Sc_{1700} = 24 \cdot 10^3$$

From the values calculated above the following matrix is obtained for

$$K = 0,079 Re^{-0,3} \cdot Sc^{-0,644} \mu$$

	A)	B)	C)	D)
1550°C	$0,04 \cdot 10^{-3}$	$0,27 \cdot 10^{-3}$	$0,39 \cdot 10^{-3}$	$1,03 \cdot 10^{-3}$
1600°C	$0,05 \cdot 10^{-3}$	$0,46 \cdot 10^{-3}$	$0,53 \cdot 10^{-3}$	$1,70 \cdot 10^{-3}$
1650°C	$0,10 \cdot 10^{-3}$	$0,76 \cdot 10^{-3}$	$1,14 \cdot 10^{-3}$	$2,85 \cdot 10^{-3}$
1700°C	$0,16 \cdot 10^{-3}$	$1,18 \cdot 10^{-3}$	$1,66 \cdot 10^{-3}$	$4,36 \cdot 10^{-3}$

Together with the viscosity data I obtained the following values for the Schmidt numbers ($Sc = \frac{\nu}{D}$):

$$Sc_{1550} = 335 \cdot 10^3$$

$$Sc_{1660} = 128 \cdot 10^3$$

$$Sc_{1650} = 52 \cdot 10^3$$

$$Sc_{1700} = 24 \cdot 10^3$$

From the values calculated above the following matrix is obtained for

$$K = 0,079 Re^{-0,3} \cdot Sc^{-0,64} u$$

	A)	B)	C)	D)
1550°C	$0,04 \cdot 10^{-3}$	$0,27 \cdot 10^{-3}$	$0,39 \cdot 10^{-3}$	$1,03 \cdot 10^{-3}$
1600°C	$0,05 \cdot 10^{-3}$	$0,46 \cdot 10^{-3}$	$0,68 \cdot 10^{-3}$	$1,70 \cdot 10^{-3}$
1650°C	$0,10 \cdot 10^{-3}$	$0,76 \cdot 10^{-3}$	$1,14 \cdot 10^{-3}$	$2,85 \cdot 10^{-3}$
1700°C	$0,16 \cdot 10^{-3}$	$1,18 \cdot 10^{-3}$	$1,66 \cdot 10^{-3}$	$4,36 \cdot 10^{-3}$

APPENDIX FOUR

Table 20 shows the composition of chromite and the reaction rim. It shows as well composition of the reaction rim in moles for the totals of 0,9, 0,7 and 0,5 mole. The columns with oxides show how much of each oxide has to go out or into the chromite to get the composition of the reaction rim for each conversion of 1 mole chromite to 0,9, 0,7 and 0,5 mole.

The number of moles for each oxide in the different total amounts was calculated from the mole percentage composition. These values were substituted from the number of moles for each oxide of the chromite for the total of 1 mole to obtain the various values of oxides.

The + means a number of moles is transferred from the chromite into the slag, the - means a flux into the chromite.

The table shows that for FeO and Cr_2O_3 there is always a flux out of the chromite, for Al_2O_3 the flux is into the chromite while the direction of the flux for MgO depends on how much reaction rim is created in its conversion from the chromite.

Approximately for the conversion 1 mole chromite to 0,62 mole reaction rim MgO goes nor in nor out.

APPENDIX FIVE

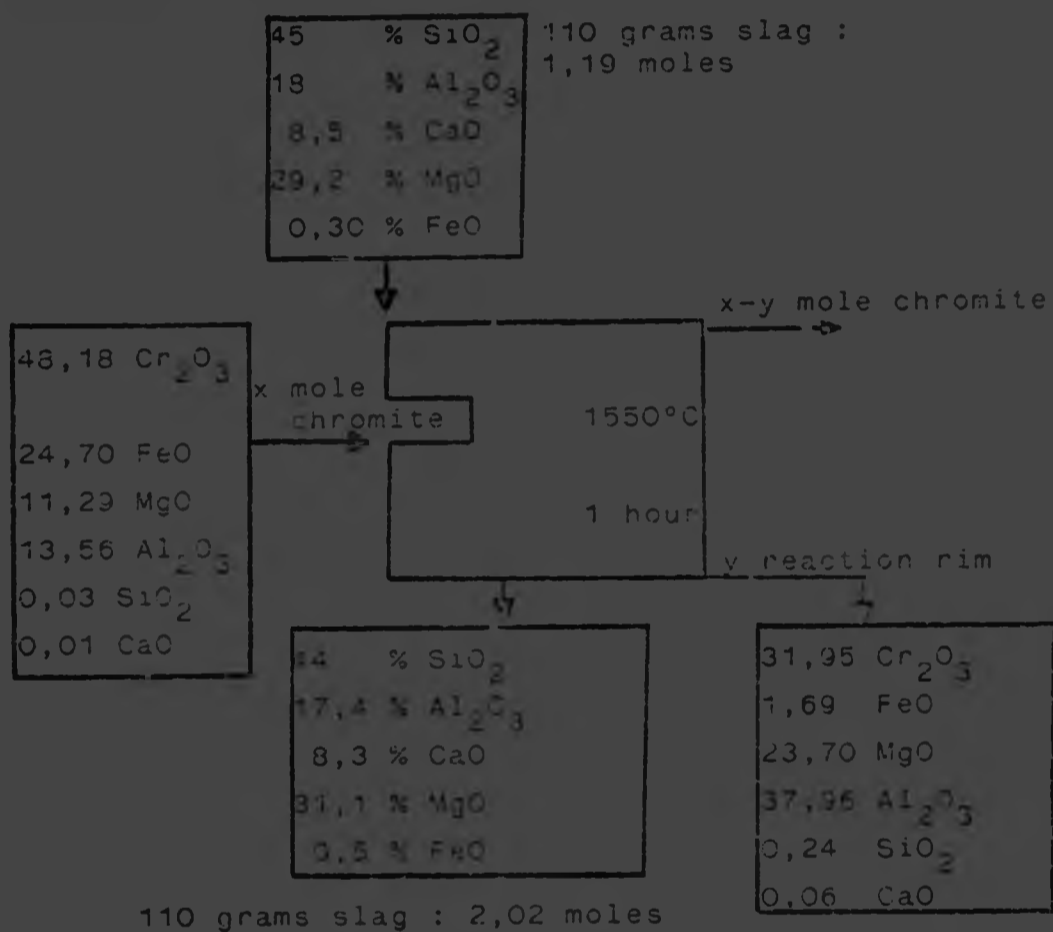
A sensitivity analysis was done on the whole system in order to investigate the feasibility of calculating the conversion factor (Y/X) of the reaction rim (x mole chromite - y mole reaction rim). In order to calculate this factor it is necessary to calculate the unknowns y and x in the following system. There exists a correlation between y and x and the percentage dissolved FeO.

mole percentage iron x total moles in the slag /
100 = moles FeO transported into the slag.
mole percentage Al_2O_3 x total moles in the slag /
100 = moles Al_2O_3 transported into the reaction
rim and the same for 11 other oxides involved
in the dissolution reaction.

These values correlate with a certain conversion factor which can be determined with a trial and error method.

It is clear that we deal with minute quantities of FeO that dissolve. In this example the FeO content goes up from 0,30% FeO - 0,5% FeO. This means FeO = 0,003 mole, MgO = 0,05 mole, SiO_2 = 0,018 mole and CaO = 0,004 mole.

FLOW DIAGRAM



SiO_2 and CaO do not take part in the dissolution process directly, are not transferred from one phase to another and, as such the number of moles should stay constant. Their change is larger though than for FeO . This sensitivity analysis shows that with the data available it is not possible to calculate a meaningful conversion factor.

TABLE 20: The compositions of chromite and reaction rim and the mass fluxes necessary to convert chromite to reaction rim (For various conversion factors)

	Mole percentages		Moles			
	Chromite	Reaction Rim	0,9 mole Oxides	0,7 mole Oxides	0,5 mole Oxides	0,5 mole oxides
Cr_2O_3	28,1%	17,5%	0,1575	0,1225	+0,1575	+0,1995
FeO	31,6%	2,5%	0,0225	+0,2975	+0,3025	+0,3075
Al_2O_3	9,6%	30,8%	0,2775	-0,1775	-0,1156	-0,084
(SiO ₂)	30,7%	49,2%	0,3628	-0,1428	-0,0444	+0,054

8 REFERENCES

- 1) Rennie, M.S. - The effects of chromium oxide, iron oxide and calcium oxide on the liquidus temperatures, viscosities and electrical conductivities of slags in the system $\text{MgO-Al}_2\text{O}_3 - \text{SiO}_2$.
Johannesburg, NIM report, No. 1423, 20 April 1972, 18 pp
- 2) Johnston, G.H.- Physicochemical properties of slags in the system $\text{MgO-Al}_2\text{O}_3 - \text{SiO}_2$ and their application to the technology of ferro-alloy smelting.
Johannesburg, NIM report, No. 1546, 13 July 1973, 25 pp
- 3) Johnston, G.H.- Physicochemical and thermodynamic properties of slags in the system $\text{MgO-Al}_{1,5} - \text{SiO}_2$.
Johannesburg, NIM report, No. 1547, 23 August 1973, 29 pp.
- 4) Urquhart, R.C - The dissipation of electrical power in the burden of a submerged arc-furnace. Johannesburg, NIM report, No. 1521, 15 February 1973, 19 pp.
- 5) Woollacott, N.L.- Factors affecting the carbon contents of alloys formed during the pre-reduction of chromite ores.
Johannesburg, NIM report, No. 1950, 31 March 1978, 24 pp.

- 6) Russell, G.M. - The spectrometric analysis of chromium bearing materials with particular reference to ferro-chromium slags and chromite ores, Johannesburg, NIM report, No. 1364, 30 November 1977, 5 pp.
- 7) Barcza, N.A. - Studies of incipient fusion in the system chromite = $MgO-Al_2O_3-SiO_2-C$. Johannesburg, NIM report, No. 1365, 5 January 1972.
- 8) Richardson, F.D. - Physical chemistry of melt in Metallurgy. 1st edition. London, Academic Press Inc. Ltd, 1974. Vol.1 p 79 - p 113
Vol. 2 p 394 - p 425.
- 9) Wadsworth, M.E. - Rate processes of extractive metallurgy. 1st edition, New York, Plenum Press, 1979, p 216 - p 244.
- 10) Szekely, J. - Rate phenomena in process metallurgy, 1st edition, New York, Wiley-Interscience, 1971, p 395 - p 454.
- 11) Bodsworth, C. & Bell, H.B. - Physical chemistry of iron and steel manufacture. 2nd edition, London, Longman Group Ltd, 1972, p 66 - p 113, p 361 - p 363.

- 12) Robiette, - Electric smelting processes, 1st
A G E edition, London, Charles Griffin
& Company Limited, 1973, p 157 -
p 159.
- 13) Evans, R C - Crystal chemistry, 2nd edition,
Cambridge University Press, 1946,
p 206 - p 211.
- 14) Rosenqvist, T - Principles of extractive.
metallurgy, 1st edition, New
York, McGraw-Hill, 1974,
p 114 - p 144.
- 15) Rankin, W J - The oxidation states of Cr in slag
and Cr distribution in slag metal
systems at 1600°C.
Trans. Inst. Min. Metal., Mar 1978,
vol C87. C60 - C70 pp.
- 16) Keller, H, - Diffusivity of Ca in CaO-SiO_2 melts.
et al Metal. Trans., Mar 1979.
- 17) Urquhart, R C - Reactions occurring during the
smelting of high carbon ferro-
chromium from Transvaal chromite
ores. Johannesburg, NIM - report,
No. 1482, 9 April 1973, 31 pp.
- 18) Waal, de, S A - The interrelation of the chemical,
physical and certain metallurgical
properties of chrome spinels from
the bushveld igneous complex,
Johannesburg, NIM report, No. 1415,
17th April 1972, 19 pp.

- 19) Waal, de, S A - The chromite of the Bushveld igneous complex. An assessment of published information, Johannesburg, NIM report, No. 1203, 1st March 1971, 28 pp.
- 20) Ellicott, J - Thermochemistry for steelmaking. Addison-Wesley Publishing Company Inc. Massachusetts, 1978, Vol. 2, pp 687 - 696.
- 21) Taylor, J - Diffusion in liquid slags. Proceedings International Symposium Metallurgical Chemistry 1971 pp 31 - 34.
- 22) Kingery, W D - Kinetics of high temperature processes. John Wiley and Sons Inc. New York, 1959, pp 80 - 85.
- 23) Geiger, G H, - Transport phenomena in metallurgy, Poirier, D R Addison-Wesley Publishing Company, Massachusetts, 1973, pp 429 - 572.
- 24) Ossin, D I - The physico chemical properties of slags associated with the production of high carbon ferrochromium and ferrochromium-silicide alloys. University of the Witwatersrand, Johannesburg, 1975, 172 pp PhD thesis.
- 25) Volkert, G, - The metallurgy of ferroalloys. et al Berlin, Springer, 1972.
- 26) Hejja, A A - Studies of factors relating to the operation and design of electric

furnaces for matte smelting with particular reference to slag characteristics. PhD Thesis, Johannesburg, 1975, pp 79 - 86.

ACOB, M. - Heat transfer, vol. 1, 1951, J Wiley, New York.

- Kinetics of deoxidation of liquid Cu-O alloys by rotating graphite cylinders under argon. Met. Trans., 108, Dec 1979, pp 659 - 658.

- The exothermic dissolution of 50 wt % ferro-silicon in molten steel. Can. Met. Quarterly, vol. 18, 1979, pp 267 - 291.

et al - Dissolution of quartz in oxide and oxide-sulfide melts. Tsvetsye Metally. pp 44 - 46

G, - Rate of dissolution of carbon in molten Fe-C alloys. Transactions of the metallurgical society of AIME Vol 236 April 1966 pp 426-429.

ACOB, M. - Phase diagrams for ceramists. Columbus, Ohio, The American Ceramic Society, 1964, 2nd edition.

A G - Ensuring the most advantageous use of platinum. Platinum Metals Review vol 23, No. 1 1970 pp 2 - 13.

- 34) Colf, van der, - Viscosities, electrical
J, et al resistivities and liquidus
temperatures of slags in the
system $\text{CaO} - \text{MgO} - \text{Al}_2\text{O}_3 -$
 $\text{TiO}_2 - \text{SiO}_2$ under neutral
conditions. Journal of
South African Inst. of Min.
and Met. April 1979 pp 255-263.
- 35) Sun, R - Diffusion of cobalt and chromium
in chromite spinel. J. Chem. Phys.,
February 1958, pp 290 - 293
- 36) Linder,,R, - Diffusion von Ni-63 in Nickelspinellen
Äkerström, Å Zeitschrift für phys. Chem., 1958,
pp 303 - 307
- 37) Lindner, R, Selbst diffusion und reaktion in
Äkerström, Å Oxyd - und Spinell system. Zeitschrift
für phys. Chem, 1956, pp 162 - 177
- 38) Himmel, L. - Selfdiffusion of iron in ironoxides
et al and the Wagner theory of oxidation
Trans. metall. Soc. AIME, June 1957.
pp 827 - 843
- 39) Dietzel, A. - Ztscher Electrochem 48 (I), 1942,
pp 9 - 23
- 40) Bockris, J.O'M The physical chemistry of melts.
Institution of Metallurgists, London.
1953, pp 9 - 15
- 41) Grimes, N.W. - Selfdiffusion of compounds with spinel
structure. Phil. Mag 25, pp 67 - 76.

9 ACKNOWLEDGEMENTS

I would like to express my gratitude towards NIM who made this work possible through their generous support. The advice, enthusiasm and co-operation of Professor D. W. Finn has contributed in a large extent to the successful completion of this work. The interest shown by Dr. S. Algie, Mr. B. McRae and A. Barnes is appreciated very much and their advice was very helpful.

I would like to thank my parents who made all this possible.

I would also like to thank my wife, Desiree Roos, for her strong support and the effort she has put into this work.

E. H. ROOS

10 RECOMMENDATIONS FOR FUTURE WORK

Considering the behaviour of magnesium and aluminium in the dissolution process it would be interesting to see the influence of the magnesium and aluminium concentration in the slag on the dissolution process.

Since aluminium plays a more dominant role in the dissolution process than magnesium it is recommended to concentrate on the first element.

Improvements to the experimental set-up are required in order to come to more accurate results. The silversteelrod and alumina rod should be replaced by a thick molybdenum rod (3-5 mm) with possibly a ring lower into the furnace, just above the crucible to hold the rod in a central position while turning. This has at the same time the advantage that the cylinder can be centered better with regard to the rod.

Preferably the chromite cylinder and the crucible are lowered together from the top of the furnace in a fixed position relative to each other, thus improving the accuracy of the set point of the immersion depth to a fraction of a millimetre.

1000

Author Roos E H

Name of thesis Measurement by use of the rotating cylinder technique of the rate of the solution of Winterveld Chromite Ore in slag 1982

PUBLISHER:

University of the Witwatersrand, Johannesburg

©2013

LEGAL NOTICES:

Copyright Notice: All materials on the University of the Witwatersrand, Johannesburg Library website are protected by South African copyright law and may not be distributed, transmitted, displayed, or otherwise published in any format, without the prior written permission of the copyright owner.

Disclaimer and Terms of Use: Provided that you maintain all copyright and other notices contained therein, you may download material (one machine readable copy and one print copy per page) for your personal and/or educational non-commercial use only.

The University of the Witwatersrand, Johannesburg, is not responsible for any errors or omissions and excludes any and all liability for any errors in or omissions from the information on the Library website.